Title: Intra-tumoral delivery of FLT3L with CXCR3/CCR5 ligands promotes XCR1+ DC1 infiltration and activates anti-tumor immunity.

Authors: Louise Gorline[1,2,3†], Fillipe Luiz Rosa do Carmo[1,2,3†], Pierre Bourdely[3,4,5], Jérémie Bornères[1,2], Nathan Vaudiau[1,2,3], Aurélie Semervil[1,2,3,4], Mathias Vetillard[3], Agathe Ok[3], Oriane Fiquet[6], Marine Andrade[6], Hannah Theobald[7], Matthieu Collin[8], Joseph Calmette[8], Giorgio Anselmi[3,9], Flavia Fico[10], Florent Ginhoux[7], Loredana Saveanu[3], Julie Helft[4], Marc Dalod[11], Mathilde Dusseaux[6], James P. Di Santo[12], Stephanie Hugues[9], Pierre Guermonprez[1,2,3*]

Affiliations

[1]Université de Paris Cité, Institut Pasteur, Immunology Department, Dendritic cells and adaptive immunity Unit, 75015 Paris, France.

[2]Université de Paris Cité, Institut Pasteur, CNRS UMR3738, Developmental Biology and Stem Cells, 75015 Paris, France.

[3]Université Paris Cité, Bichat Medical School, INSERM UMR1149, CNRS EMR8252, 75018 Paris, France.

[4]Université Paris Cité, Institut Cochin, INSERM UMR 1016, CNRS UMR 8104, 75014 Paris, France.

[5]Laboratory of Tumor Inflammation and Angiogenesis, Center for Cancer Biology, VIB, Leuven.

[6]Human Disease Models Core Facility, Institut Pasteur, Université Paris Cité, 75015 Paris, France.

[7]Gustave Roussy, Inserm U1015, Université Paris-Saclay, Villejuif, France.

[8]Inserm Transfert, 7 rue watt, 75013 Paris, France.

[9]Radcliffe Department of Medicine, MRC Molecular Haematology Unit, MRC Weatherall Institute of Molecular Medicine, University of Oxford, Oxford, UK.

[10]Department of Pathology and Immunology, Geneva Medical School, Geneva, Switzerland.

[11]Aix Marseille Univ, CNRS, INSERM, CIML, Centre d'Immunologie de Marseille-Luminy, France.

[12]Institut Pasteur, Immunology Department, Immunité Innée, 75015 Paris, France.

[†]These authors contributed equally to this work.

*Corresponding author: pierre.guermonprez@pasteur.fr

Abstract

Tumor infiltration by dendritic cells (DCs) has been identified as a biomarker associated with favorable outcomes and improved responses to immunotherapies by T cell immune checkpoint blockade. However, tumor induced immunosuppressive pathways contrive efficient DC infiltration. This calls for the development of DC-targeted interventions purposed to stimulate DC infiltration and local expansion. Here we deliver a proof-of-concept for a cell-based immunotherapeutic approach promoting circulating DC progenitors infiltration in the tumor together with their local expansion. We report that engraftment of autologous mesenchymal stromal cells engineered to express the membrane bound form of FLT3L (eMSC-FLT3L) uniquely induce DC infiltration, T cells activation and anti-tumor immunity, when combined with an adjuvant like the poly(I:C) double stranded RNA mimic. Mechanistic experiments demonstrate that poly(I:C)-induced CXCR3 and CCR5 ligands (CXCL9, CCL5) are required for intra-tumoral DC and T cell recruitment and for the therapeutic effect of eMSC-FLT3L + poly(I:C) immunotherapy. Stromal cell-based delivery of CXCL9 and CCL5, together with FLT3L, by-passes the requirement for poly(I:C) agonist and is sufficient to induce T cell and DC recruitment within tumors. These findings are transferrable to human settings as we show that eMSCs-FLT3L-CXCL9-CCL5 stimulate tissue infiltration by human XCR1^{+} DC1s in mice harboring a 'Human Immune System' (HIS mice). Lastly, we report that engraftment of eMSC-FLT3L-CXCL9-CCL5 in the tumor induces anti-tumor immunity and partially overcomes resistance to immune checkpoint blockade. Altogether, these data support the therapeutic potential of expanding intra-tumoral DC1s using a continuous and local source of FLT3L, CXCL9 and CCL5.

One sentence summary: Intra-tumoral delivery of FLT3L synergizes with CXCL9 and CCL5 to activate the expansion of intra-tumoral DCs.

Main Text:

INTRODUCTION

An important factor limiting the development of anti-tumor immunity lies in the extent of tumor infiltration by immune cells, including dendritic cells (DCs). DCs are sentinel cells of the immune system initiating the tumor-immunity cycle (*1*, *2*).

Tumor-associated DCs (TADCs) up-take antigens by phagocytosis and migrate to tumor draining lymph nodes (tdLNs) after up-regulating CCR7. If engaged in immunogenic maturation by the activation of proper innate signalling pathways, DCs can prime anti-tumor $CD4^+$ and $CD8^+$ T cells in tdLNs (*2*, *3*). Once activated, effector T lymphocytes can migrate back to tumors *via* efferent lymph and then blood (*2*). All these activities define DCs as initiators of the cancer-immunity cycle.

In addition to this virtuous cycle of T cell activation in tdLN, intra-tumoral DCs also have local roles. Indeed, they participate to the recruitment of $CXCR3^+$ effector T cells via the release of CXCL9 chemokines (*4–6*). Also, intra-tumoral DCs shape niches supporting the survival of tumor-infiltrating T cells (TILs) by delivering specific trophic cues. For instance, $CXCL16^+$ TADCs attract $CXCR6^+TCF1^-$ effector and promote their survival by trans-presenting IL15 (*7*). DCs establish local interactions with $CD28^+$ T cells and preserve their fitness (*8*). Finally, $CCR7^+$ $LAMP3^+$ DCs also populate Tertiary Lymphoid Structures (*9*), some "stem immunity hubs" related-lymphoid aggregates where they colocalize with $TCF1^+CD8^+$ TILs (*6*, *10*) and establish some tripartite interactions with $CXCL13^+CD4^+$ T cells and $TCF1^+CD8^+$ TILs (*11*).

DCs are classified into two major subsets: $XCR1^+$ type 1 DCs (DC1s), which express IRF8 and an heterogenous population of $CD11b^+$ DCs expressing IRF4 and encompassing DC2s and DC3s. DC1s play a non-redundant role in the rejection of immunogenic tumors (*12*) and are essential for the efficacy of immune checkpoint blockade (ICB) therapies, as demonstrated in pre-clinical models (*13*, *14*). Furthermore, DC1 infiltration in human tumors correlates with favorable clinical outcomes and response to ICB (*15*, *16*). Mechanistically, DC1 would fine tune the $CD8^+$ T cell response by maintaining the pool of $TCF1^+$ TILs along tumor development thereby fueling a reservoir of T cells potentially promoting effector anti-tumor responses (*17*). However, DC1s infiltration within tumors remains generally limited (*18*) (*19*, *20*). COX enzymes in tumor cells limit the activation of NK-dependent DCs recruitment (*16*) (*21*). Also, oncogenic pathways such as β-catenin limit the recruitment of DC1s by limiting

92 CCL4 production (*20*). Therefore, enhancing the recruitment and activation of intra-tumoral
93 DC1s remains an unmet therapeutic need to overcome cancer-induced immune suppression.
94 Mechanistically, recruitment of circulating DCs have been investigated in the context
95 of pre-clinical models of immunogenic tumors (*15*, *20*, *21*). Böttcher *et al.* have identified that
96 DC1s recruitment depends on NK-cell derived CCR5 ligands (CCL4, CCL5), as well as XCR1
97 ligands (XCL1, XCL2) (*21*). It is unclear if infection activated CCR2-dependent pathways (*22*)
98 also control DC1s recruitment.
99 The FLT3L-FLT3 signalling pathway is essential for the homeostasis of conventional
100 DCs, including DC1s, in both mice (*23*, *24*) and humans (*25*). Intra-tumoral FLT3L is an
101 important biomarker associated to the density of TADCs, particularly DC1s, in human
102 melanoma (*15*). FLT3L-FLT3 pathway supports DC development and maintenance in both
103 lymphoid organs and peripheral tissues (*23*). Tissue FLT3L supports the proliferation of DC
104 precursors (pre-DCs) in bone marrow and peripheral sites (*23*, *26*). Of note, radio-resistant cells
105 control homeostatic levels of FLT3L (*27*). Within secondary lymphoid organs, stromal cells
106 contribute to DC pool maintenance. For example, a $CCL19^{+}GREMLIN^{+}$ fibroblastic niche
107 support DCs survival at homeostasis (*28*) via FLT3L production (*29*). However, the cellular
108 sources of FLT3L within tumors are not very well known. Barry *et al.* have shown that NK
109 cells represent a substantial source of FLT3L (*15*) but other sources like T cells (*30*) or mast
110 cells (*27*) might participate to local FLT3L production.
111 Administration of recombinant soluble FLT3L is an effective approach to expand
112 circulating DCs (*31*) in humans but it faces questionable safety issues with general modification
113 of hematopoiesis and expansion of tolerogenic DCs (*32*). Furthermore, systemic recombinant
114 FLT3L might promote immune tolerance, as it leads to the expansion of regulatory T cells (*33*)
115 (*34*). Lastly, combination therapies of FLT3L with innate agonists such as anti-CD40 (*19*) or
116 poly(I:C) (*14*) raise some toxicity concerns associated to systemic inflammation.
117 Here, we have reasoned that targeted, local interventions in the tumor microenvironment
118 (TME) could optimize local generation of immunogenic DCs (*35*), while avoiding most
119 systemic effects underpinning immune regulation or toxicity. Here, we explore the therapeutic
120 potential of delivering engineered autologous stromal cells within the TME. Engrafted stromal
121 cells are expressing chemotactic factors supporting DC infiltration, differentiation, proliferation
122 and maintenance. We identify that stromal membrane bound form of FLT3L combined to
123 poly(I:C) or CXCL9 and CCL5 is sufficient to activate the local recruitment and accrual of
124 DC1s, T and NK/ILC1 cells within tumors. Furthermore, we show that these immunotherapies
125 stimulate anti-tumor immunity and partially overcome resistance to ICB. Altogether, these

126 findings open a new avenue to rewire the tumor microenvironment by local cell-based
127 therapeutic intervention.

128 **RESULTS**

129 **Intra-tumoral delivery of engineered mesenchymal stromal cells expressing membrane**
130 **bound FLT3L does not alter intra-tumoral and systemic DC1 populations**

131 We have previously demonstrated that engineered stromal cells expressing human FLT3L act
132 as "synthetic niches" able to support the differentiation of human tissue DCs in
133 immunodeficient mice (*36*). In a first attempt to stimulate intra-tumoral DCs accumulation, we
134 generated stable, autologous, fibroblastic cell lines from embryonic fibroblasts of C57BL/6
135 mice and termed as engineered mesenchymal stromal cells thereafter (eMSC). eMSC-FLT3L
136 express homogeneously the membrane form of human FLT3L, as detected by flow cytometry
137 (Fig. **1A**). We found that eMSC-FLT3L but not eMSC-Control (eMSC-Ctrl) stimulated the
138 differentiation of DC1s and DC2s, when co-injected with CD45.1 bone-marrow hematopoietic
139 stem cell progenitors (HSPCs) in basal membrane extract plugs in the dermis of tumor free
140 mice, showing that FLT3L expressed in eMSC-FLT3L was functional (Fig. **1B-C, S.1A**). On
141 the contrary, rec-huFLT3L did not stimulate DC differentiation within the plugs. We next
142 decided to inject eMSC-FLT3L within subcutaneous B16 melanoma tumors expressing
143 ovalbumin (B16-OVA), which have a primary resistance to immune checkpoint blockade
144 (ICB). First, we found that $gp38^{+}GFP^{+}$ eMSC-FLT3L were still detectable on site 14 days after
145 intra-tumoral injection, validating their persistence within the TME (Fig. **1D-E**). We next
146 compared intra-tumoral engraftment of eMSC-FLT3L to B16F10 cells overexpressing human
147 FLT3L (B16-huFLT3L) and assessed their impact on DCs differentiation. In contrast with B16-
148 huFLT3L, B16F10 tumor bearing mice that had received intra-tumoral engraftment of eMSC-
149 FLT3L at day 7 did not display an elevation of systemic FLT3L serum levels at day 12 (Fig.
150 **1F-G**). However, we did not observe an increase of DC1s in the tumor (Fig. **1H**), lymph node
151 (Fig. **1I**) nor spleen (Fig. **1J**).

152 We conclude that intra-tumoral injection of eMSC-FLT3L does not alter intra-tumoral and
153 systemic DC1 populations.

154

155 **Intra-tumoral delivery of eMSC-FLT3L synergizes with poly(I:C) to activate anti-tumor**
156 **immunity**

157 We next wondered if innate agonist administration would circumvent the inability of eMSC-
158 FLT3L to expand intra-tumoral DCs. We chose to use poly(I:C) because it had previously been
159 shown to stimulate anti-tumor immunity in combination with recombinant, soluble FLT3L (*14*).
160 We designed our intra-tumoral cell-based therapy as two injections of eMSC-FLT3L and one
161 injection of poly(I:C) within B16-OVA tumors (Fig. **1K**). We found that only eMSC-FLT3L in
162 combination with poly(I:C) induced tumor regression as assessed by the tumor growth (Fig.

163 **1L**) and the tumor weight (Fig. **1M**). In addition, the combination therapy extended the survival
164 of mice. Importantly, 10% of the mice treated with the combination therapy eliminated the
165 tumor without relapses until day 90 (Fig. **1N**). In a clinical translational point of view, we asked
166 if adult, autologous fibroblasts would represent a suitable option for eMSC-based
167 immunotherapy. To test this, we generated a $CD45^{-}CD31^{-}$ stromal fraction from adult murine
168 visceral and inguinal adipose tissues. We transduced them to express membrane bound human
169 FLT3L (eAMSC-FLT3L) (Fig. **1O**). Following the same experimental plan as previously
170 described (Fig. **1K**), we found that eAMSC-FLT3L displayed similar efficiency as eMSCs-
171 FLT3L, when combined with poly(I:C), as showed by the reduced tumor growth (Fig. **1P**) and
172 tumor weight (Fig. **1Q**).
173 We conclude that adult fibroblasts are amenable to engineering for local immunotherapy.
174 Altogether, these experiments show that local cell-based delivery of FLT3L within the TME in
175 combination with poly(I:C) is a potent therapy to control tumor growth.

Fig1. Intra-tumoral engraftment of autologous mesenchymal stromal cells expressing membrane bound FLT3L stimulates anti-tumor immunity in the presence of poly(I:C)

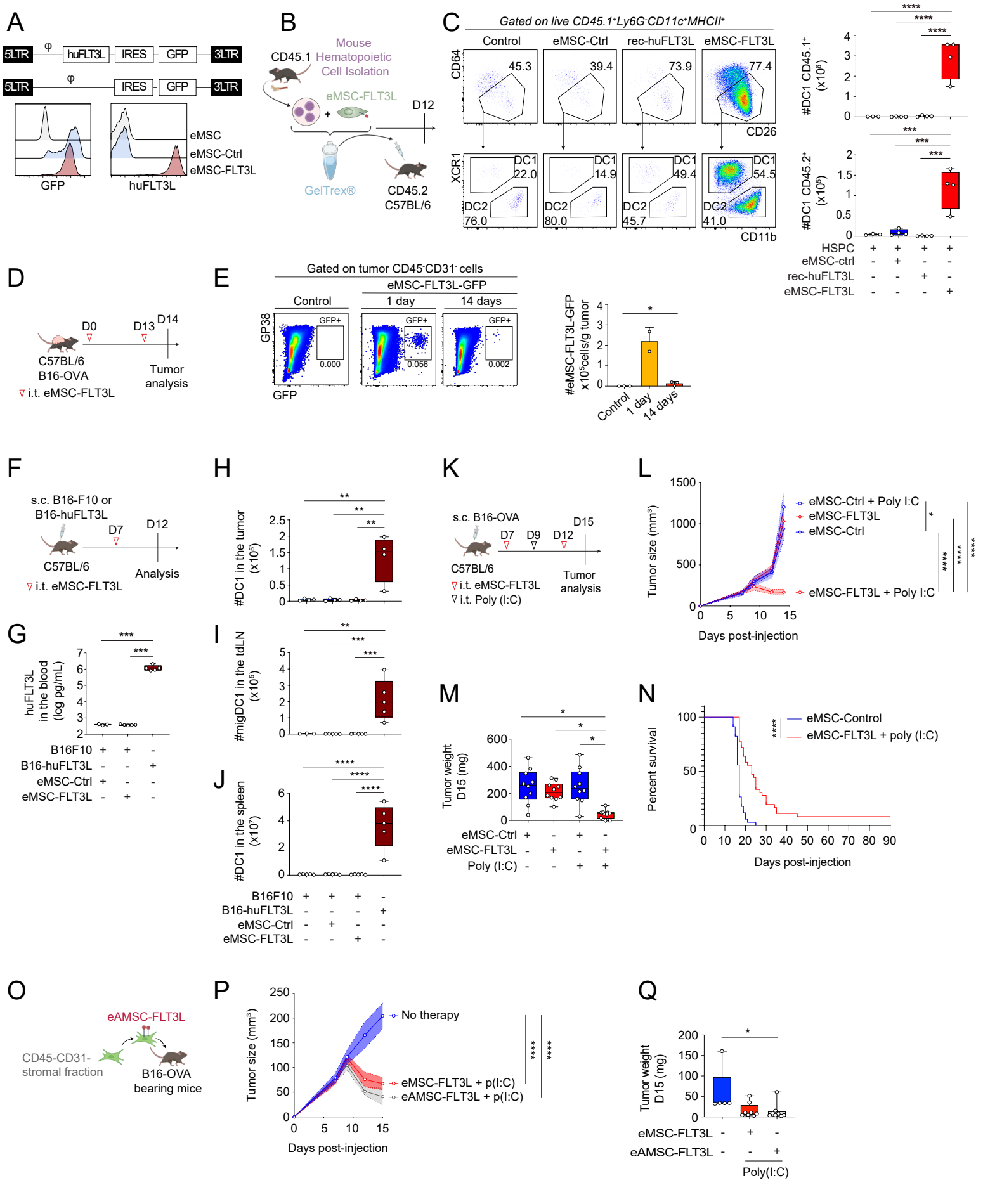

176

177 **<u>Figure 1:</u> Intra-tumoral engraftment of autologous mesenchymal stromal cells expressing**
178 **membrane bound FLT3L stimulates anti-tumor immunity in the presence of poly(I:C)**
179 **(A)** Expression of GFP (eMSC-Ctrl) and human membrane-bound FLT3 ligand in mouse
180 embryonic fibroblasts (eMSC-FLT3L).
181 **(B)** Experimental design to assess the ability of eMSC-FLT3L to drive DCs differentiation *in*
182 *vivo*. Hematopoietic stem and progenitor cells (HSPCs) isolated from $CD45.1^+$ bone marrow
183 cells were injected subcutaneously (s.c.) in $CD45.2^+$ C57BL/6 mice, along with eMSC-FLT3L,
184 eMSC-Ctrl, recombinant huFLT3L or alone, in a basement membrane extract preparation
185 (Geltrex®). These synthetic niches were harvested and analyzed by flow cytometry 12 days
186 after the injection.
187 **(C)** Representative flow cytometry plots and quantification of CD45.1 and CD45.2 DC1s in the
188 synthetic niches containing eMSC-FLT3L, eMSC-Ctrl, rec-huFLT3L or alone at day 12. (n =
189 4 plugs per group, one experiment. ***$p < 0.001$, ****$p < 0.0001$, one-way ANOVA-test with
190 Tukey's multiple comparisons).
191 **(D)** Experimental design to evaluate the persistence of eMSC-FLT3L within B16-OVA tumors.
192 $5x10^5$ eMSC-FLT3L-GFP were injected in the tumor (i.t.) at day 0 and at day 13 for the positive
193 controls. Tumors were harvested at day 14 and analyzed by flow cytometry.
194 **(E)** Representative flow cytometry plots and quantification of the absolute number of eMSC-
195 FLT3L-GFP/g tumor. Number of cells was checked in B16-OVA tumors, 24h and 14 days after
196 eMSC-FLT3L-GFP injection in the tumor. (n = 2-3 mice per group, one experiment, *$p < 0.05$,
197 one-tailed Mann-Whitney test).
198 **(F)** Experimental design to evaluate DCs subsets in tumors, tumor-draining lymph nodes and
199 spleens. Mice were injected subcutaneously (s.c.) with B16F10 or B16-huFL3L-GFP on day 0.
200 At day 7, eMSC-Ctrl or eMSC-FLT3L were injected into the tumor (i.t.). DC1s were analyzed
201 at day 12 in the indicated organs.
202 **(G)** Circulating huFLT3L levels measured by ELISA in mice serum at day 12. (n=5 mice per
203 group in one experiment. ***$p < 0.001$, one-way ANOVA-test with Tukey's multiple
204 comparisons).
205 **(H, I, J)** Quantification of the absolute numbers of DC1s in the tumors (H), in the skin tumor-
206 draining lymph nodes (I) and in the spleens (J) (n = 4-5 mice per group, one experiment. **$p <$
207 0.01, ***$p < 0.001$, ****$p < 0.0001$, one-way ANOVA-test with Tukey's multiple
208 comparisons).
209 **(K)** Experimental design to evaluate anti-tumoral effects of eMSC-FLT3L and poly(I:C) in
210 B16-OVA melanoma mice model. Mice were injected subcutaneously (s.c.) with B16-OVA on

211 day 0. At day 7 and 12, mice were injected into the tumor (i.t.) with eMSC-FLT3L or eMSC-
212 Ctrl. At day 9, mice were treated i.t. with poly(I:C).
213 **(L-M)** Tumor growth curves (L) and tumor weight at day 15 (M) (n=10 mice per group, two
214 independent experiments, *p < 0.05, **p < 0.01, ***p < 0.001, ****p < 0.0001, Kruskal-
215 Wallis' test with Dunn's multiple comparisons, two-way ANOVA-test with Tukey's multiple
216 comparisons test).
217 **(N)** Survival curves. (n=34-36 mice per group in six independent experiments, ****p < 0.0001,
218 log-rank (Mantel-Cox) test)
219 **(O)** Experimental design. Adipocytes precursors (CD45-CD31-) were isolated from inguinal
220 and visceral fat of C57BL/6 mice and transduced with human membrane-bound FLT3 ligand.
221 These transduced cells were then injected in the tumor of B16-OVA bearing mice, following
222 the experimental design in (K).
223 **(P)** Tumor growth curves. (A line represents the mean and SD is shown with the colored area,
224 n=5 no therapy and n=8 mice for the two other groups in one experiment, ****p < 0.0001 two-
225 way ANOVA-test with Dunnett's multiple comparisons)
226 **(Q)** Tumor weight at day 15. (*p < 0.05, Kruskal-Wallis' test with Dunn's multiple
227 comparisons).

228 **Intra-tumoral delivery of eMSC-FLT3L and poly(I:C) stimulates the infiltration of DC1s,**
229 **that are required for immunotherapy efficiency**
230 Having established the immunotherapeutic potential of eMSC-FLT3L + poly(I:C) combination,
231 we next sought to address if this intervention would modify DCs infiltration in the TME. To do
232 so, we injected twice eMSC-FLT3L in B16-OVA tumors and we analysed the tumor DCs 24h
233 or 6 days after a poly(I:C) injection (Fig. **2A**). We observed that 24 hours post poly(I:C)
234 injection (day 10), tumor DC1s underwent phenotypic maturation, as probed by CD40 and
235 CD86 up-regulation within both eMSC-Ctrl and eMSC-FLT3L deliveries (Fig. **2B-C**).
236 Poly(I:C) injection also induced a decrease in the number of DC1s in both eMSC-Ctrl and
237 eMSC-FLT3L treated tumors (Fig. **2C**). In contrast, 6 days post poly(I:C) injection (day 15)
238 DC1s underwent expansion in mice treated with both poly(I:C) and eMSC-FLT3L but not in
239 mice treated with poly(I:C) or eMSC-FLT3L alone (Fig. **2C**). This shows that sustained DC1s
240 expansion at the tumor site, uniquely achieved by the synergy of eMSC-FLT3L and poly(I:C),
241 correlates with the efficiency of the therapy. Of note, similar results were found for DC2s (Fig.
242 **S2A**). In order to test the role of DC1s in the efficiency of the therapy, we injected B16-OVA
243 in WT and in DC1-deficient mice (*Xcr1*$^{cre/+}$ *Rosa*$^{lsl\text{-}DTA}$ (*37*)) and treated the tumors with eMSC-
244 FLT3L and poly(I:C) immunotherapy. We found that the tumor control (Fig. **2D**) and the
245 survival extension (Fig. **2E**) provided by the therapy, were totally abrogated in the absence of
246 DC1s.
247 We conclude that the synergy between eMSC-FLT3L and poly(I:C) expands intra-tumoral
248 DC1s, that are required for the therapeutic benefits of this intervention.

Fig2. DC1s expand upon intra-tumoral delivery of eMSC-FLT3L with poly(I:C) and control tumor growth.

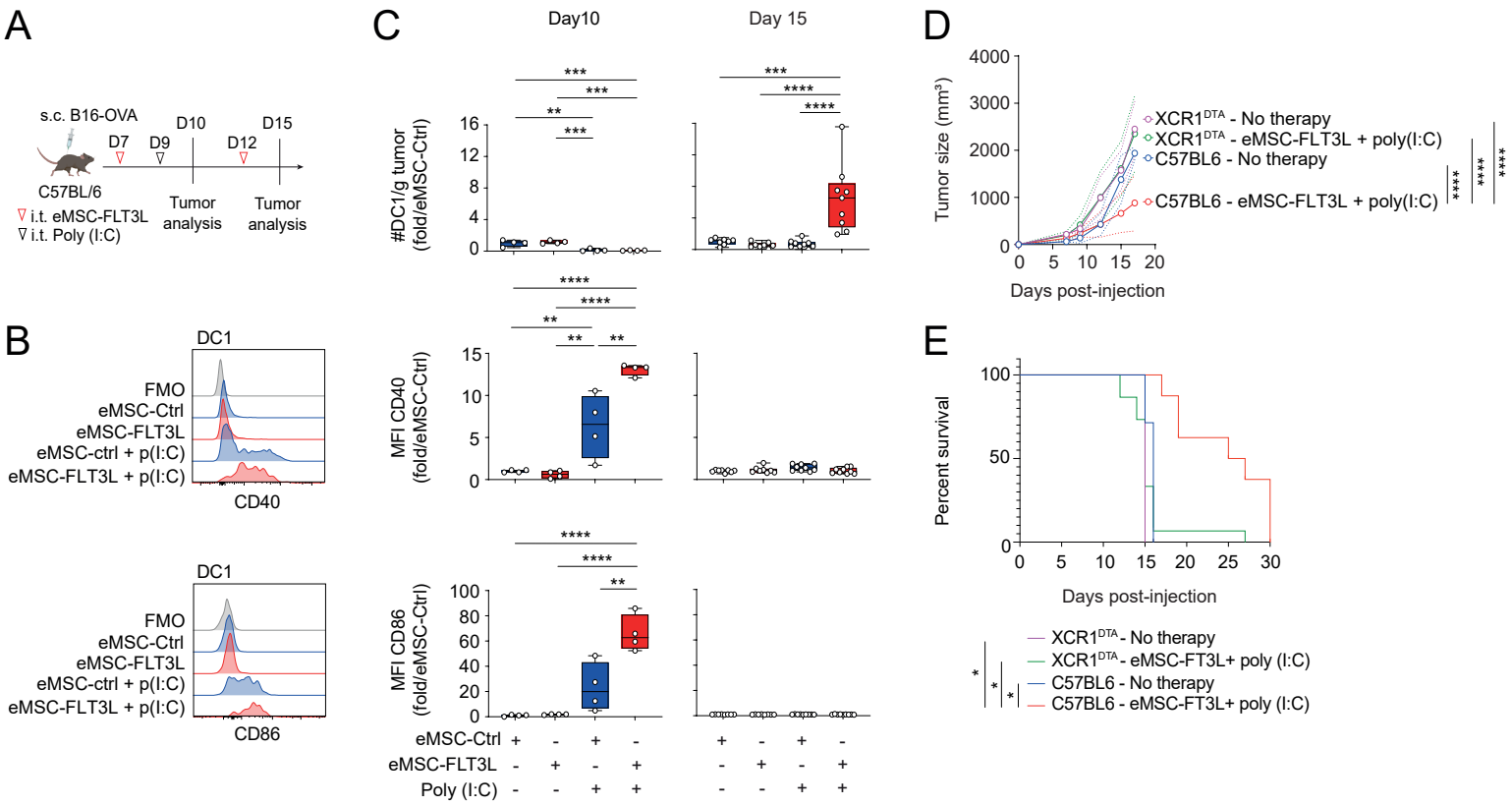

249

<u>Figure2:</u> DC1s expand upon intra-tumoral delivery of eMSC-FLT3L with poly(I:C) and control tumor growth.

(A) Experimental design to evaluate DC1s infiltration in B16-OVA upon injection of eMSC-FLT3L + poly(I:C). Mice were injected subcutaneously (s.c.) with B16-OVA on day 0. At day 7 and 12, mice were injected into the tumor (i.t.) with eMSC-FLT3L or eMSC-Ctrl. At day 9, mice were treated i.t. with poly(I:C). Tumors were harvested at day 10 and 15 for flow cytometry analysis.

(B-C) Representative flow cytometry plots at day 10 (B) and quantification (C) of the absolute number of intra-tumoral DC1/g tumor and the mean fluorescence intensity (MFI) of CD40 and CD86. Results are shown as fold change to control (eMSC-Ctrl). (n=4 mice per group, one experiment for day 10, n=8-9 mice per group, two independent experiments for day 15, **$p < 0.01$, ***$p < 0.001$, ****$p < 0.0001$, one-way ANOVA-test with Tukey's multiple comparisons).

(D) Tumor growth curves of $XCR1^{DTA}$ mice or C57BL/6 WT mice treated or not with eMSC-FLT3L + poly(I:C). (A line represents the mean and SD is shown with the colored doted lines, n=4 mice $XCR1^{DTA}$ - No therapy and n=8 mice for the three other groups, one experiment, ****$p < 0.0001$ two-way ANOVA-test with Tukey's multiple comparisons).

(E) Survival curves. (n=4 mice $XCR1^{DTA}$ - No therapy and n=8 mice for the three other groups, one experiment, *$p < 0.05$, log-rank (Mantel-Cox) test).

Intra-tumoral delivery of eMSC-FLT3L and poly(I:C) increase mature migratory DC1 in tumor-draining lymph nodes

Having identified DC1s anti-tumor role in our therapeutic approach, we next wondered if this effect relied on tumor-draining lymph nodes (tdLNs). As previously, we injected twice eMSC-FLT3L in B16-OVA tumors and we analysed the tdLNs 24 hours (day 10) and 6 days (day 15) after the poly(I:C) administration (Fig. **3A**). At 24 hours post poly(I:C) injection, we observed an increase in the migration of mature ($CD40^{high}$, $CD86^{high}$) DC1s in the tdLNs of tumors treated with poly(I:C) (Fig. **3B-C**). 6 days post poly(I:C) injection, we found that the increase of mature migratory DC1s was restricted to the tdLNs of tumors treated with eMSC-FLT3L and poly(I:C) (Fig. **3C**).

In correlation with the expansion and activation of intra-tumoral DC1s previously observed (Fig. **2C**), we conclude that the eMSC-FLT3L and poly(I:C) immunotherapy promotes the migration of mature DC1s in the tumor-draining lymph node.

Intra-tumoral delivery of eMSC-FLT3L and poly(I:C) enables cross-priming of tumor-specific $CD8^+$ T cells

Since DC1s are more mature and play a crucial role in the therapy, we investigated whether there was an induction of the adaptive immune response in the tdLN. At day 15, we found that the absolute number of activated $CD8^+$ T cells increased upon eMSC-FLT3L and poly(I:C) therapy (Fig. **3D-E**). This effect was associated with an increase in proliferation, as probed by Ki67 staining, in both $TCF1^+CD44^+$ stem-like $CD8^+$ and more differentiated $TCF1^-TIM3^+$ T cells (Fig. **3D-F**). Functionally, $CD8^+$ T cells increased their capacity to secrete IFN-γ and effector to T regulatory cells (Tregs) ratio increased (Fig. **3G, S.3A-B**). Interestingly, we observed a significant increase in the absolute number of $CD4^+Foxp3^-$ cells but not in Tregs (**Fig. S3B-C**). Furthermore, CD4+Foxp3- cells of tumors treated with eMSC-FLT3L and poly(I:C) increased their secretion of IFN-γ (Fig. **S.3D**). Finally, the eMSC-FLT3L and poly(I:C) immunotherapy induced the expansion of tumor specific $CD8^+$ T cells that recognize the $OVA_{257-264}$ immunodominant peptide, as shown with the tetramer staining (Fig. **3H**). Altogether, we conclude that the therapeutic efficiency of eMSC-FLT3L and poly(I:C) associates with increased cross-priming of anti-tumor $CD8^+$ T cells.

Fig3. Intra-tumoral delivery of eMSC-FLT3L and poly(I:C) increase mature migratory DCs in tumor-draining lymph nodes and enables cross-priming of tumor-specific CD8+ T cells.

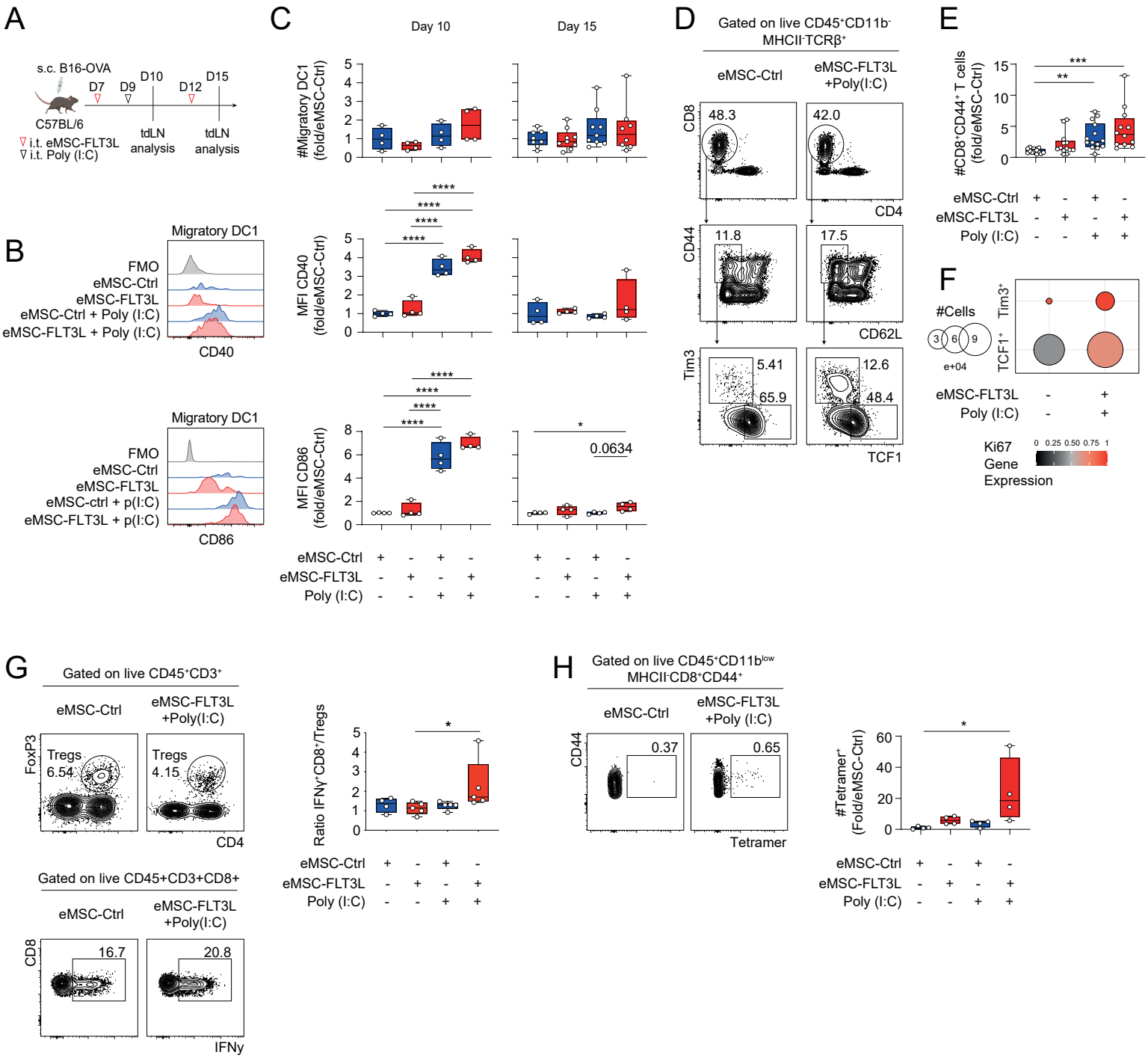

299

<u>Figure3:</u> Intra-tumoral delivery of eMSC-FLT3L and poly(I:C) increase mature migratory DCs in tumor-draining lymph nodes and enables cross-priming of tumor-specific CD8$^+$ T cells.

(A) Experimental design to evaluate migratory DC1 in the tumor-draining lymph node upon intra-tumoral injection of eMSC-FLT3L + poly(I:C). Mice were injected subcutaneously (s.c.) with B16-OVA on day 0. At day 7 and 12, mice were injected into the tumor (i.t.) with eMSC-FLT3L or eMSC-Ctrl. At day 9, mice were treated i.t. with poly(I:C). Tumor-draining lymph nodes were harvested at day 10 and day 15 for flow cytometry analysis.

(B-C) Representative flow cytometry plots at day 10 (B) and quantification (C) of the absolute number of migratory DC1s and the mean fluorescence intensity (MFI) of CD40 and CD86. Results are shown as fold change to control (eMSC-Ctrl). (n=4-8 mice per group in one or two independent experiment, *$p < 0.05$, ****$p < 0.0001$, one-way ANOVA with Dunnett's multiple comparisons test, Kruskal-Wallis-test with Dunn's multiple comparisons).

(D) Representative flow cytometry plots of CD8 T cells in the tumor-draining lymph node at day 15.

(E) Quantification of the absolute number of activated T cells. Results are shown as fold change to control (eMSC-Ctrl). (n=12-14 mice per group, three independent experiments, **$p < 0.01$, ***$p < 0.001$ Kruskal-Wallis test with Dunn's multiple comparisons).

(F) Quantification of the absolute number and Ki67 expression of exhausted (Tim3$^+$) and stem-like (TCF1$^+$) T cells. Dots represent the absolute number of cells while the colours represent the expression level of Ki67. (n=4 mice per group).

(G) Representative flow cytometry plots and quantification of the ratio of IFNγ$^+$CD8$^+$ T cells over T regulatory cells at day 15. (n=5 mice per group in one experiment, *$p < 0.05$, Kruskal-Wallis test with Dunn's multiple comparisons).

(H) Representative flow cytometry plots and absolute number quantification of OVA-specific CD8$^+$ Tetramer$^+$ T cells at day 15. Results are shown as fold change to control (eMSC-Ctrl)**.** (n=4 mice per group, representative of two independent experiments, *$p < 0.05$, one-way ANOVA-test with Tukey's multiple comparisons).

328 **Intra-tumoral delivery of eMSC-FLT3L and poly(I:C) stimulates the infiltration of T and**
329 **NK cells within tumor beds, that are required for immunotherapy efficiency**
330 We next wondered if eMSC-FLT3L and poly(I:C) immunotherapy had an impact on the
331 infiltration of intra-tumoral lymphocytes. First, we characterized lymphoid infiltrates at day 15
332 within B16-OVA tumors, treated with eMSC-FLT3L and poly(I:C) (Fig. **4A**). We found that
333 eMSC-FLT3L and poly(I:C) synergized to expand intra-tumoral NK1.1^{+} conventional NK cells
334 (cNK) and CD62L^{-}CD49a^{+} type 1 innate lymphoid cells (ILC1) (Fig. **4B-C**). We also observed
335 an increase in the proliferation of these two cell types, as probed by Ki67 staining (Fig. **4B-C**).
336 Furthermore, we noticed an increase in intra-tumoral CD8^{+} T cells (Fig. **4D-E**) and CD4^{+} T
337 cells (Fig. **S.4A**). By looking closer to the phenotype of the activated tumor infiltrating
338 lymphocytes (T_{ACT}), we found that eMSC-FLT3L + poly(I:C) immunotherapy increased both
339 PD1^{+}TIM3^{+} CD8^{+} exhausted T cells (T_{EX}) and TIM3^{-}TCF1^{+}CD8^{+} progenitor exhausted T cells
340 (T_{PEX}) (Fig. **4D-E**). Of note, the intra-tumoral abundance of T_{PEX} is associated to responses to
341 immunotherapy in multiple cancer types (*38–40*). Interestingly, expansion of T_{PEX} cells was
342 associated to a massive increase in cell cycling activity, as probed by Ki67 staining (Fig. **4D-**
343 **E**). By contrast, T_{EX} cells displayed a high cycling activity both in control and treated groups.
344 Strikingly, the abundance and cycling activity of intra-tumoral T regulatory cells (Tregs) was
345 not up-regulated by eMSC-FLT3L + poly(I:C) immunotherapy (Fig. **S.4A-B**). We next
346 wondered whether these changes would associate to increased tumor-antigen-specific T cell
347 response. We found that eMSC-FLT3L + poly(I:C) immunotherapy induced a striking
348 expansion of tumor specific CD8^{+} T cells for the $OVA_{257-264}$ peptide, as detected by the tetramer
349 staining (Fig. **4F**) and the IFNγ -secreting T cells upon peptide-specific (SIINFEKL) *ex-vivo*
350 restimulation (Fig. **4G**). Having established the local infiltration of tumor-specific T cells
351 during the onset of tumor growth, we next wondered if the few survivor mice that had
352 undergone eMSC-FLT3L + poly(I:C) immunotherapy displayed evidence of tumor-specific T
353 cell memory. To test this, we injected the SIINFEKL synthetic peptide in tumor-free or B16-
354 OVA survivor mice (d90 post primary tumor injection) (Fig. **4H**). We found that this re-
355 challenge induced the expansion of CD8^{+} T cells specific for the $OVA_{257-264}$-H2K^{b} complex
356 (Fig. **4I**) in inguinal lymph nodes from survivor mice but not from tumor free naïve mice.
357 Furthermore, those CD8^{+} T cells displayed a circulating effector memory phenotype (Fig. **4J**).
358 We conclude that eMSC-FLT3L + poly(I:C) immunotherapy induce local, systemic and long-
359 term immunity against tumor antigens in the CD8^{+} T cell compartment. Finally, in order to
360 probe the requirement for conventional CD4 and CD8 T cells as well as NK cells, we performed
361 eMSC-FLT3L + poly(I:C) immunotherapy in the presence of control, NK1.1 or CD4 and CD8

362 depleting antibodies, alone or in combinations (Fig. **4K**). We found that both NK and CD4/CD8
363 contributed to the therapeutic effect of eMSC-FLT3L + poly(I:C), as probed by the reversed
364 inhibition of the tumor growth (Fig. **4L**) and of the extension of survival (Fig. **4N**). Importantly,
365 inhibition of both NK and CD4/CD8 T cells achieved the maximal inhibition of eMSC-FLT3L
366 + poly(I:C) immunotherapy.
367 Altogether, we conclude that eMSC-FLT3L + poly(I:C) immunotherapy activates and relies on
368 both innate and adaptive anti-tumor immune response.
369

370 **Intra-tumoral delivery of eMSC-FLT3L and poly(I:C) overcomes resistance to anti-**
371 **PD1/CTLA-4 immune checkpoint blockade**

372 Lastly, we wondered if stimulation of T and NK-dependent anti-tumor immunity by eMSC-
373 FLT3L and poly(I:C) immunotherapy would by-pass resistance to immune checkpoint
374 blockade (ICB). To test this, we submitted B16-OVA to aPD1/aCTLA-4 ICB immunotherapy
375 (Fig. **4O**). We found that ICB slightly expanded the survival of mice as compared to isotype
376 control-treated mice. However, mice treated with both ICB and eMSC-FLT3L + poly(I:C)
377 immunotherapies exhibited a significant reduction of tumor growth (Fig. **4P**) and had extended
378 survival as compared to isotype-treated control groups (Fig. **4Q**). Of note, the combination of
379 both ICB and eMSC-FLT3L + poly(I:C) improved eMSC-FLT3L + poly(I:C) alone in terms of
380 survival, indicating a proper synergistic effect between both interventions.
381 Altogether, these data indicate that eMSC-FLT3L + poly(I:C) immunotherapy induce T and
382 NK-dependent immunity against B16-OVA tumor and this defines a way to partially overcome
383 resistance to ICB immunotherapy.

Fig4. Intra-tumoral delivery of eMSC-FLT3L and poly(I:C) stimulates the infiltration of T and NK cells within tumor beds that are required for immunotherapy efficiency and overcomes primary resistance to PD1/CTLA4 blockade.

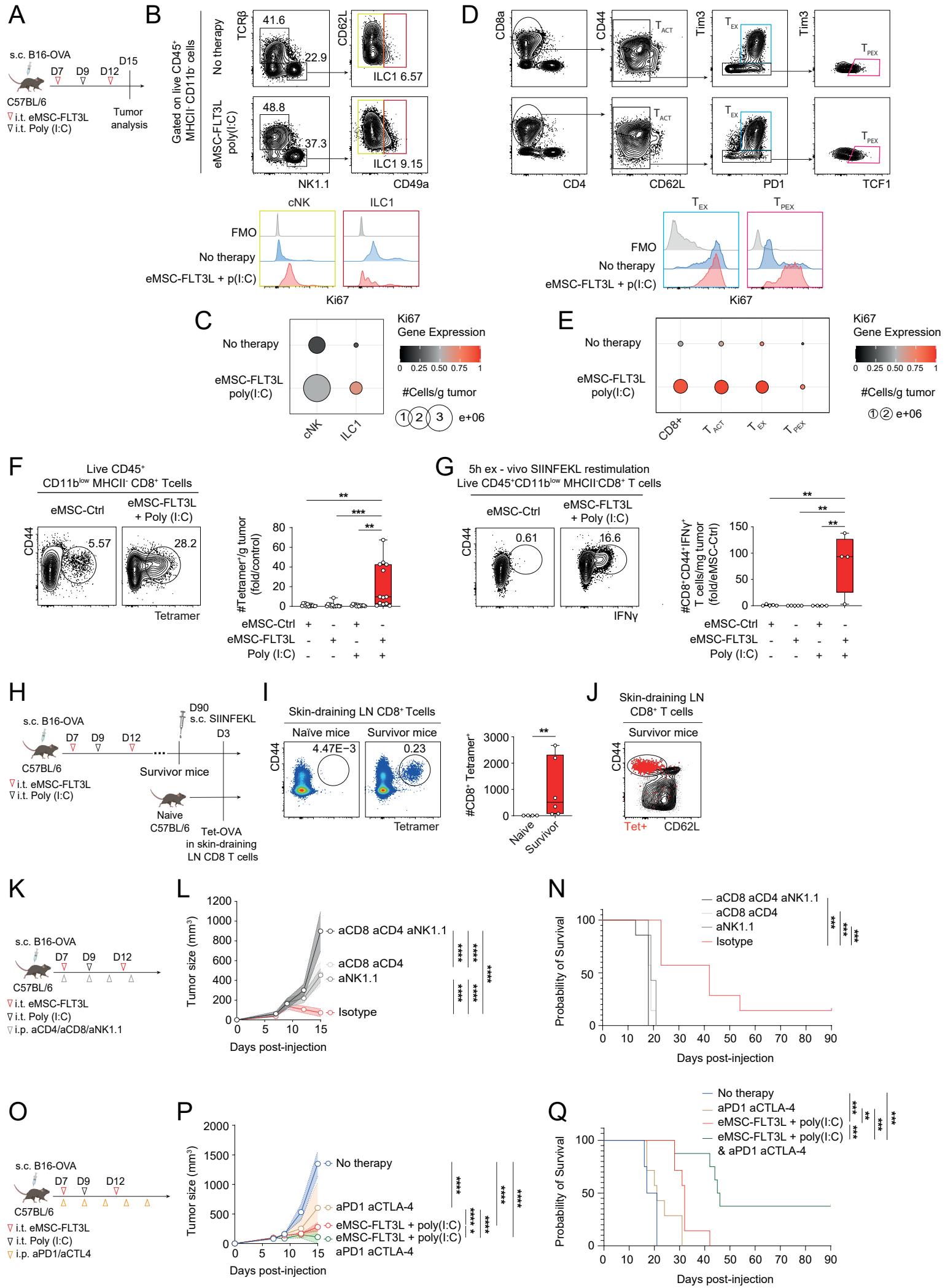

385 **<u>Figure 4:</u> Intra-tumoral delivery of eMSC-FLT3L and poly(I:C) stimulates the**
386 **infiltration of T and NK cells within tumor beds that are required for immunotherapy**
387 **efficiency and overcomes primary resistance to PD1/CTLA4 blockade.**
388 **(A**) Experimental design to evaluate T and NK cells infiltration in B16-OVA upon injection of
389 eMSC-FLT3L + poly(I:C). Mice were injected subcutaneously (s.c.) with B16-OVA on day 0.
390 At day 7 and 12, mice were injected into the tumor (i.t.) with eMSC-FLT3L. At day 9, mice
391 were treated i.t. with poly(I:C). Tumors were harvested at day 15 for flow cytometry analysis.
392 **(B-C)** Representative flow cytometry plots (B) and quantification (C) of NK1.1 and ILC1
393 subsets. Dots represent the absolute number of cells while the colours represent the expression
394 level of Ki67. (n=4 mice per group, one experiment).
395 **(D-E)** Representative flow cytometry plots (D) and quantification (E) of activated (T_{ACT}),
396 progenitor exhausted (T_{PEX}) and exhausted (T_{EX}) $CD8^+$ T cells. Dots represent the absolute
397 number of cells/g tumor while the colours represent the expression level of Ki67. (n=4 mice per
398 group, one experiment)
399 **(F)** Representative flow cytometry plots and absolute number quantification of OVA-specific
400 $CD8^+$ $Tetramer^+$ T cells/g tumor. Results are shown as fold change to control (eMSC-Ctrl)**.**
401 (n=12-14 mice per group, three independent experiments, **$p < 0.01$, ***$p < 0.001$, Kruskal-
402 Wallis' test with Dunn's multiple comparisons).
403 **(G)** Representative flow cytometry plots and absolute number quantification of
404 $IFN\gamma^+CD44^+CD8^+$ T cells/g tumor after 5h ex-vivo restimulation with SIINFEKL. Results are
405 shown as fold change to control (eMSC-Ctrl)**.** (n=4-5 mice per group, one experiment, **$p <$
406 0.01, Kruskal-Wallis' test with Dunn's multiple comparisons).
407 **(H)** Experimental design to evaluate T cell memory generation. Survivor mice that fully
408 rejected B16-OVA tumor treated with eMSC-FLT3L and poly(I:C) were re-challenged, 90 days
409 after primary tumor injection, with s.c. SIINFEKL (1µg/per mice) at the tumor site. Naïve mice
410 were injected s.c. with SIINFEKL as control. At day 3 after SIINFEKL challenge, skin-draining
411 lymph nodes were analyzed.
412 **(I)** Representative flow cytometry plots and quantification of $CD44^+CD8^+Tetramer^+$ cells in the
413 skin-draining lymph nodes after *in vivo* SIINFEKL OVA-peptide restimulation. (n=4 naïve and
414 n=6 survivor, **$p < 0.01$, two-tailed Mann-Whitney test).
415 **(J)** Representative flow cytometry plots of $Tet^+OVA^+CD8^+$ T cells (red dots) overlaid on total
416 $CD8^+$ T cells of the survivor mice.
417 **(K)** Experimental design to assess the role of CD4, CD8 and NK cells in the anti-tumor effect
418 induced by eMSC-FLT3L + poly(I:C) treatment. Mice were injected subcutaneously (s.c.) with
419 B16-OVA on day 0. At day 7 and 12, mice were injected into the tumor (i.t.) with eMSC-

420 FLT3L. At day 9, mice were treated i.t. with poly(I:C). Tumors were treated 4 times with
421 intraperitoneally injection of anti-CD4, anti-CD8, anti-NK1.1 ab or control IgG, every two days
422 starting at day 7.
423 **(L)** Tumor growth curves. (A line represents the mean and SD is shown with the colored area,
424 n=7 mice per group, one experiment, ****$p < 0.0001$, two-way ANOVA-test with Tukey's
425 multiple comparisons).
426 **(N)** Survival curves. (n=7 mice per group, one experiment, ***$p < 0.001$, log-rank (Mantel-
427 Cox) test).
428 **(O)** Experimental design to evaluate the response of tumors treated with eMSC-FLT3L +
429 poly(I:C), together with immune checkpoint blockade. Mice were injected subcutaneously (s.c.)
430 with B16-OVA on day 0. At day 7 and 12, mice were injected into the tumor (i.t.) with eMSC-
431 FLT3L. At day 9, mice were treated i.t. with poly(I:C). Tumors were treated 5 times with
432 intraperitoneally injection of anti-PD-1 and anti-CTLA-4, every two days starting at day 7.
433 **(P)** Tumor growth curves. (A line represents the mean and SD is shown with the colored area,
434 n=7-8 mice per group, one experiment, *$p < 0.05$, ****$p < 0.0001$, two-way ANOVA-test with
435 Tukey's multiple comparisons).
436 **(Q)** Survival curves. (n=7-8 mice per group, one experiment, **$p < 0.01$, ***$p < 0.001$, log-
437 rank (Mantel-Cox) test).

438 **CXCR3 and CCR5 ligands are induced by poly(I:C) and control its impact on DC1s and**
439 **T cells infiltration**

440 We next wondered which mechanism induced by poly(I:C) could explain the synergy between
441 eMSC-FLT3L and poly(I:C). Since eMSC-FLT3L alone are able to recapitulate DCs
442 development from hematopoietic progenitors when engrafted in the dermis of tumor free mice
443 (Fig. **1C, S.1A**), we asked whether eMSC-FLT3L would also recapitulate DC development
444 from DC progenitors within the TME. To test this, we engrafted eMSC-FLT3L together with
445 bone marrow hematopoietic stem and progenitors cells (HSPCs), containing DC precursors and
446 obtained from CD45.1 mice, within B16-OVA tumors (Fig. **5A**). 3 days after the engraftment
447 of HSPCs, we found that CD45.1^{+} DC1s had differentiated from progenitors co-engrafted with
448 eMSC-FLT3L but not eMSC-Ctrl (Fig. **5B**). In the same tumors, eMSC-FLT3L did not increase
449 DC1s from the recipient mice, consistently with previous results (Fig. **5C**). We conclude that
450 availability of DC precursors and not specific features of the TME restrict the differentiation of
451 pre-DC into DC1s within B16-OVA tumors. We next wondered if poly(I:C) would regulate the
452 infiltration of pre-DC1s via chemokine regulation. Using a chemokine multiplex array, we
453 found that poly(I:C) up-regulated multiple chemokines within the TME of eMSC-FLT3L-
454 treated tumors (Fig. **5D**). This includes CXCL9 and CXCL11, which both act as ligands for the
455 CXCR3 receptor, and CCL5, that acts as ligand for CCR5 (*41*) (Fig. **5E**). CXCR3 and CCR5
456 are found on activated T and NK cells but also on circulating DC precursors (*42*) (*43*) (*44*). To
457 test the contribution of these chemokine signalling pathways to the eMSC-FLT3L + poly(I:C)
458 therapy, we treated B16-OVA bearing mice receiving the therapy with CXCR3 and/or CCR5
459 antagonists (Fig. **5F**). We found that CXCR3 and CCR5 inhibition prevented the anti-tumoral
460 impact of eMSC-FLT3L + poly(I:C) immunotherapy, as shown with the tumor growth (Fig.
461 **5G**) and the tumor weight (Fig. **5H**). Furthermore, blockade of CXCR3 and/or CCR5 inhibited
462 the accrual of intra-tumoral DC1s (Fig. **5I**) and the increase of activated CD8^{+} T cells within
463 tdLN (Fig. **5J**).

464 Altogether, these data highlight the crucial role of CXCR3 and CCR5 signalling pathways in
465 mediating the immunotherapeutic effect of eMSC-FLT3L + poly(I:C) immunotherapy.

Fig5. CXCR3 and CCR5 ligands are induced by poly(I:C) and control its impact on DC1s and T cells infiltration.

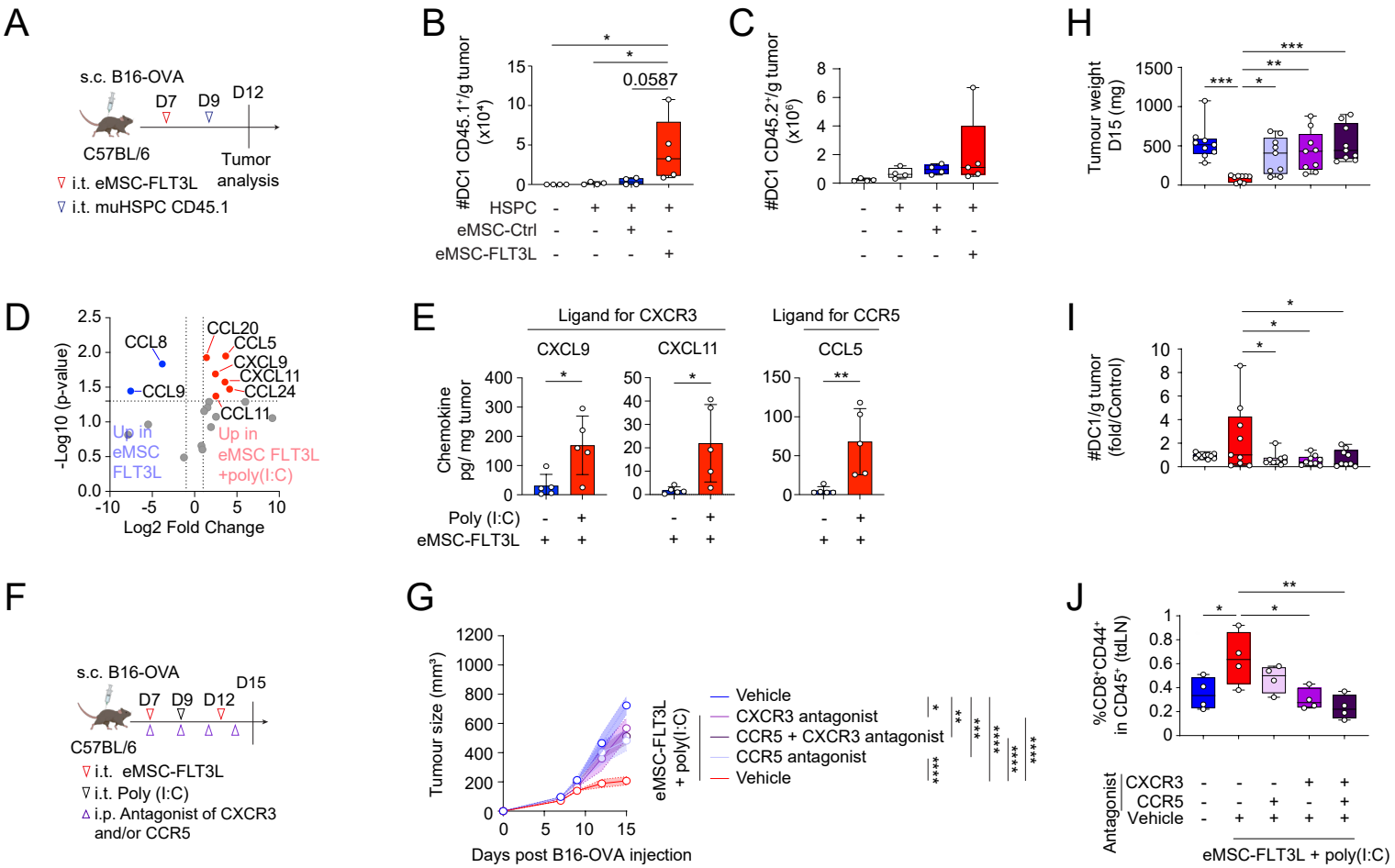

466

467 **<u>Figure 5:</u> CXCR3 and CCR5 ligands are induced by poly(I:C) and control its impact on**
468 **DC1s and T cells infiltration.**
469 **(A)** Experimental design to assess the ability of eMSC-FLT3L to drive DCs differentiation in
470 B16-OVA tumors. CD45.2^{+} C57BL/6 mice were injected subcutaneously (s.c.) with B16-OVA
471 on day 0. At day 7, mice were injected into the tumor (i.t.) with eMSC-FLT3L. At day 9,
472 Hematopoietic Stem and Progenitor Cells (HSPCs) isolated from CD45.1^{+} bone marrow cells
473 were injected into the tumors. Tumors were harvested and analyzed by flow cytometry 3 days
474 after HSPCs injection.
475 **(B-C)** Quantification of the absolute number of CD45.1 DC1/g tumor (B) and CD45.2 DC1/g
476 tumor (C) (n = 4-5 mice per group in one experiment. *p < 0.05, one-way ANOVA test with
477 Dunnett's multiple comparisons).
478 **(D)** Volcano plot for the chemokine multiplex array, where each dot represents one gene,
479 plotted based on log2 fold change and –log10 of adj p-value. Genes in blue are up-regulated in
480 tumors treated with eMSC-FLT3L, while genes in red are up-regulated in tumors treated with
481 eMSC-FLT3L + poly(I:C).
482 **(E)** Individual selected chemokines of interest, based on up-regulated chemokines in eMSC-
483 FLT3L + poly(I:C) found in volcano plot. Values were obtained with a Legendplex. (n=5 mice
484 per group, one experiment, *p < 0.05, **p < 0.01, two-tailed Mann–Whitney test).
485 **(F)** Experimental design to block chemokine receptors CXCR3 and/or CCR5. Mice were
486 injected subcutaneously (s.c.) with B16-OVA on day 0. At day 7 and 12, mice were injected
487 into the tumor (i.t.) with eMSC-FLT3L. At day 9, mice were treated i.t. with poly(I:C). Tumors
488 were treated 4 times with intraperitoneal injection of CXCR3- and CCR5 antagonists or of
489 vehicle, every two days starting at day 7. Tumors were harvested at day 15 and analyzed by
490 flow cytometry.
491 **(G)** Tumor growth curves. A line represents the mean and SD is shown with the colored area.
492 (n=9, two independent experiments, *p < 0.05, **p < 0.01, ***p < 0.001, ****p < 0.0001, two-
493 way ANOVA-test with Tukey's multiple comparisons).
494 **(H)** Tumor weight at day 15. (n=9, two independent experiments, *p < 0.05, **p < 0.01, ***p
495 < 0.001, Kruskal-Wallis test with Dunn's multiple comparisons).
496 **(I)** Quantification of the absolute number of DC1/g tumor. Results are shown as fold change to
497 control (DMEM + vehicle)**.** (n=9-10 mice per group, two independent experiments, *p < 0.05,
498 one-way ANOVA test with Dunnett's multiple comparisons).

499 **(J)** Quantification of the frequency of activated $CD8^+$ T cells in live $CD45^+$ cells in the tumor-
500 draining lymph node. (n=4 mice per group, one experiment, *$p < 0.05$, ** < 0.01, one-way
501 ANOVA test with Dunnett's multiple comparisons).

502 **Intra-tumoral delivery of eMSC co-expressing FLT3L, CXCL9 and CCL5 stimulates the**
503 **infiltration of immature pre-DC1s and DC1s in WT and BRGSF Human Immune System**
504 **(HIS) mice**
505 We next reasoned that stromal cell-based delivery of CXCL9 and/or CCL5 could substitute the
506 effect of poly(I:C) on eMSC-FLT3L therapy. To test this, we produced eMSCs engineered to
507 express CCL5 or CXCL9 (Fig. **6A**) that secrete high concentrations of both chemokines in
508 culture (Fig. **6B-C**). Then, we asked whether eMSC-FLT3L-CXCL9-CCL5 would allow the
509 entry of circulating pre-DC1s within B16-OVA tumors. To test this, we injected IRF8-GFP
510 reporter mice with 2 tumors on either flank and injected eMSC-FLT3L on one side (left) and
511 eMSC-FLT3L-CXCL9-CCL5 on the other side (right) (Fig. **6D**). IRF8-GFP mice are useful to
512 identify IRF8-expressing pre-DC1s and DC1s. 24h after the injection, we found that CCL5 and
513 CXCL9 enriched tumors had an increased infiltration of pre-DC1s, as defined by Lin-
514 CD45RB^{+}FLT3^{+}MHCII^{+}CD26^{+}Ly6C^{-}CD172a^{-} XCR1^{-} IRF8^{high}SIRPa^{-} cells (Fig. **6E**). We next
515 wondered if this infiltration of pre-DC1s would translate into local DC1s expansion at later time
516 points post-treatment. We found that tumors that were treated with eMSC-FLT3L-CXCL9-
517 CCL5 had an increase both in the absolute number (Fig. **6F**) and the frequency (Fig. **6G**) of
518 DC1s. Furthermore, we noticed that upon the therapy, tumor DC1s tend to be more activated,
519 as shown by CD40 up-regulation (Fig. **6H**). Altogether, these data show that stromal cells
520 expressing CXCL9 and CCL5 can substitute the effect of poly(I:C) on DCs recruitment and
521 maturation. We then wondered if the eMSC-FLT3L-CXCL9-CCL5 co-localized with DC1s in
522 the tumors. We injected eMSC-FLT3L-CXCL9-CCL5 (both Cherry^{+} and GFP^{+}) in
523 *Xcr1*^{cre}x*Rosa*^{LsLRFP} mice, in which DC1s are genetically labelled with RFP fluorescence. We
524 found that DC1s established contact with eMSC-FLT3L-CXCL9-CCL5 at the border of tumor
525 sites (Fig. **6I**). Since CCR5 and CXCR3 (*4*) are expressed by activated T and NK cells, we
526 wondered if the infiltration of pre-DC1s/DC1s was indirect, due to the recruitment, at first, of
527 activated lymphoid cells. To test this, we used BRGS mice that are deficient in murine T and B
528 cells *(Rag2*$^{-/-}$*),* murine NK cells *(IL-2Rγ*$_c^{-/-}$) -and macrophage phagocytosis of human cells
529 (SIRPα^{NOD}). (*45*) BRGS mice were injected subcutaneously with basal membrane extract plugs
530 containing either eMSC-Ctrl (left flank), or eMSC-huFLT3L-CCL5-CXCL9 (right flank). (Fig.
531 **6J**). We found that eMSC-FLT3L-CXCL9-CCL5 triggered a local accumulation of DC1s in
532 the absence of lymphocytes. We next wondered if this response was actually dependent on the
533 FLT3 receptor tyrosine kinase that is required for the homeostasis of tissue DC1s in non-
534 lymphoid tissues (*23*). To test this, we used BRGSF mice deficient in FLT3 (BRGSF *Flt3*$^{-/-}$)
535 (*46*).We observed no DC1s recruitment in mice deficient in tissue DCs, both in control and
536 treated plugs (Fig. **6K**). From these results, we conclude that the recruitment of DC1 induced

537 by eMSC-FLT3L-CXCL9-CCL5 is independent on B, T and NK/ILCs cells but dependent on
538 FLT3 signalling. Finally, we wondered whether our findings would be transferable to human
539 settings. To test this in controlled experimental settings, BRGSF mice were engrafted with
540 $CD34^+$ HSPCs from human cord blood to create HIS mice.17-weeks old BRGSF HIS mice
541 showed multi-lineage human immune reconstitution comprising B, T, NK and DC.
542 Reconstituted BRGSF HIS mice were injected subcutaneously with basal membrane extract
543 plugs containing either eMSC-Ctrl (left flank), or eMSC-FLT3L-CXCL9-CCL5 (right flank)
544 (Fig. **6L**). After 10 days, mice were sacrificed and the cellular infiltrates populating the plugs
545 in the dermis of the mice were analysed by flow cytometry. We found that plugs containing
546 eMSC-FLT3L-CXCL9-CCL5 had a significant increase in human DC1s (Fig. **6M**), as
547 compared to plugs containing eMSC-Ctrl eMSC-containing plugs, both in absolute number
548 (Fig. **6N**) and frequency (Fig. **6O**). Of note, similar trends were observed for human DC2s (Fig.
549 **S5A-B**).
550 Altogether, we conclude that the engraftment of eMSC expressing FLT3L, CXCL9 and CCL5
551 represent an efficient platform to promote the recruitment and expansion of DC1s within tissues
552 and that the system is amenable to human DC1s.

Fig6. Intra-tumoral delivery of eMSC co-expressing FLT3L, CXCL9 and CCL5 stimulates DC1s infiltration in mice and humanized mice.

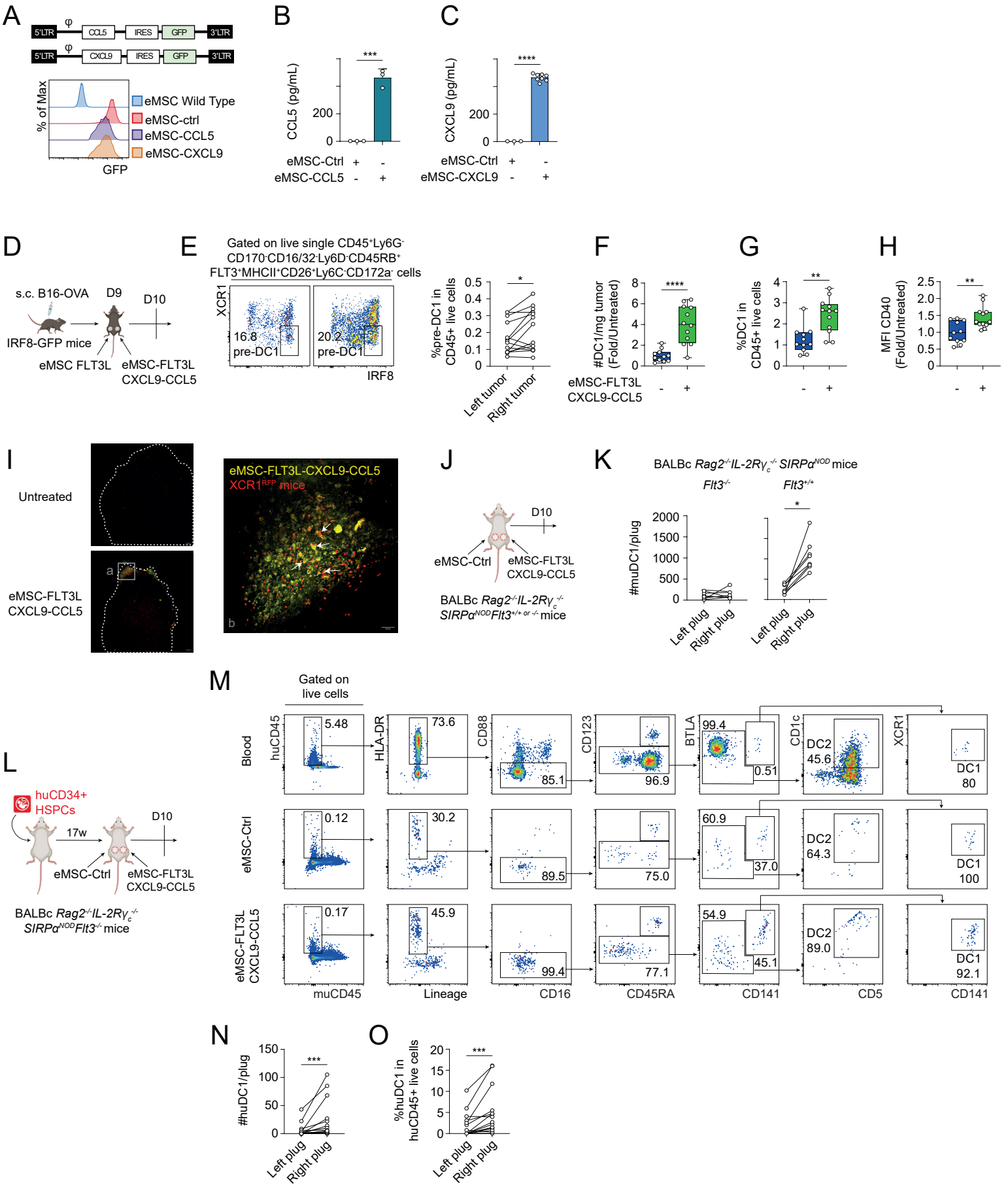

553

554 **<u>Figure 6:</u> Intra-tumoral delivery of eMSC co-expressing FLT3L, CXCL9 and CCL5**
555 **stimulates DC1s infiltration in mice and humanized mice.**
556 **(A)** Expression of GFP in the mouse embryonic fibroblasts control (eMSC-Control) and in the
557 one expressing CCL5 (eMSC-CCL5) or CXCL9 (eMSC-CXCL9).
558 **(B-C)** Quantification by ELISA of CCL5 (B) and CXCL9 (C) released by the eMSC. (n=3 for
559 the eMSC-Ctrl and the eMSC-CCL5 and n=8 for the eMSC-CXCL9 in one experiment, ***p
560 < 0.001, ****p < 0.0001, two-tailed unpaired t-test).
561 **(D)** Experimental design to evaluate the ability of eMSC-FLT3L-CXCL9-CCL5 to recruit pre-
562 DC1s in the tumor. IRF8-GFP mice were injected subcutaneously (s.c.) with two B16-OVA
563 tumors on day 0. At day 9, mice were injected with eMSC-FLT3L in the left tumor and with
564 eMSC-FLT3L-CXCL9-CCL5 in the right tumor. Tumors were harvested after 24h and
565 analyzed by flow cytometry.
566 **(E)** Representative flow cytometry plots and frequencies of immature pre-DC1s upon $CD45^+$
567 live cells in the tumors. (n=14, three independent experiments, *p < 0.05, two-tailed paired t-
568 test).
569 **(F-H)** Quantification by flow cytometry of the absolute number of DC1/g tumor (F), their
570 frequency in $CD45^+$ live cells (G) and their mean fluorescence intensity (MFI) of CD40 (H) at
571 day 15, after 3 intra-tumoral injections of eMSC-FLT3L-CXCL9-CCL5. Results (F, H) are
572 shown as fold change to control (Untreated). (n=11-12 mice per group, two independent
573 experiments, **p < 0.01, ****p < 0.0001, two-tailed unpaired t-test).
574 **(I)** Immunofluorescence imaging of YUM-OVA tumors injected in XCR1-cre-ROSA-RFP
575 mice. These tumors received 3 injections of DMEM (Untreated) or eMSC-FLT3L-CXCL9-
576 CCL5. Images were taken with a spinning disk 24h after the last injection. DC1 are in red, while
577 eMSC-FLT3L-CXCL9-CCL5 are in yellow. Tumors are delimited with the doted white lines.
578 **(J)** Experimental design to evaluate the recruitment of murine DC1s in tissues in *BALB/c, Rag2*$^{-}$
579 $^{/-}$, *IL-2Rγ*$_c^{-/-}$, *SIRPα*^{NOD}, *Flt3*$^{+/+\ or\ -/-}$ (BRGS and BRGSF) mice. eMSC-Ctrl or eMSC-FLT3L-
580 CXCL9-CCL5 were injected subcutaneously (s.c.) in BRGSF mice in two independent
581 basement membrane extract preparation (GelTrex®). These synthetic niches (plugs) were
582 harvested and analyzed by flow cytometry 10 days after the injection.
583 **(K)** Quantification of the absolute number of murine DC1/plug in BRGS *Flt3*$^{-/-}$ or *Flt3*$^{+/+}$ mice.
584 (n=8 plugs per group, one experiment, ***p < 0,05, two-tailed paired t-test)
585 **(L)** Experimental design to evaluate the recruitment of human DC1s in tissues in *BALB/c, Rag2*$^{-}$
586 $^{/-}$, *IL-2Rγ*$_c^{-/-}$, *SIRPα*^{NOD}, *Flt3*$^{-/-}$ (BRGSF) humanized mice. eMSC-Ctrl or eMSC-FLT3L-
587 CXCL9-CCL5 were injected subcutaneously (s.c.) in BRGSF mice in two independent

588 basement membrane extract preparation (GelTrex®). These synthetic niches (plugs) were
589 harvested and analyzed by flow cytometry 10 days after the injection.
590 **(M)** Representatives flow cytometry plots and gating strategy used to identify human DC1 in
591 the synthetic niches. Lineage contains: NKp46, CD3, CD19, CD56, CD66b, CD203c, CD20.
592 **(N-O)** Quantification of the absolute number (N) and frequencies (O) of human DC1/plug.
593 (n=16 plugs per group, three independent experiments, ***$p < 0.001$, two-tailed Wilcoxon
594 matched-pairs signed rank test).

595 **Intra-tumoral delivery of eMSC co-expressing FLT3L, CXCL9 and CCL5 stimulates the**
596 **infiltration of activated CD4 and CD8 T cells in the tumor**
597 We next wondered if the secretion of CXCL9 and CCL5 would also impact the attraction of
598 activated T cells. To test this, we first set-up an *in vitro* migration assay in Boyden chambers,
599 to study the chemo-attraction of activated polyclonal $CD4^+$ and $CD8^+$ T cells towards eMSCs
600 expressing CCL5 and/or CXCL9 (Fig. **7A**). As expected, after 3 hours of migration, we
601 observed a synergistic effect of eMSC-CCL5 and eMSC-CXCL9 in their ability to attract
602 activated $CD4^+$ (Fig. **7B**) and $CD8^+$ T cells (Fig. **7C**). We then wanted to know if this attraction
603 could allow the recruitment of activated T cells in B16-OVA tumors. To test this, we injected
604 eMSC expressing CCL5 and/or CXCL9 in the tumors and adoptively transferred *ex vivo*
605 activated polyclonal CD45.1 T cells intravenously (Fig. **7D**). A synergistic effect between
606 eMSC-CCL5 and eMSC-CXCL9 was again observed in their ability to recruit activated $CD4^+$
607 (Fig. **7E**) and $CD8^+$ (Fig. **7F**) CD45.1 T cells in the tumor. We conclude that eMSC-CXCL9
608 and eMSC-CCL5 represent a workable platform to deliver locally bioactive chemokines.
609 Lastly, we wanted to assess if the eMSC-FLT3L-CXCL9-CCL5 immunotherapy would have
610 an impact on the infiltration of intra-tumoral lymphocytes. To test this, we injected eMSC-
611 FLT3L-CXCL9-CCL5 in B16-OVA tumors and looked at a late time point the immune
612 infiltrate (Fig. **7G**). We observed that tumors treated with eMSC-FLT3L-CXCL9-CCL5 were
613 more infiltrated with NK, ILC1, $CD4^+$ and $CD8^+$ T cells (Fig. **7H**). Of note, absolute number
614 of activated, exhausted and progenitor exhausted $CD8^+$ T cells were also increased in the treated
615 tumors.
616 Altogether these data show that eMSC-FLT3L-CXCL9-CCL5 immunotherapy induce the
617 recruitment of lymphoid cells in B16-OVA tumors.

Fig7. Intra-tumoral delivery of eMSC co-expressing FLT3L, CXCL9 and CCL5 stimulates the infiltration of activated CD4+ and CD8+ T cells.

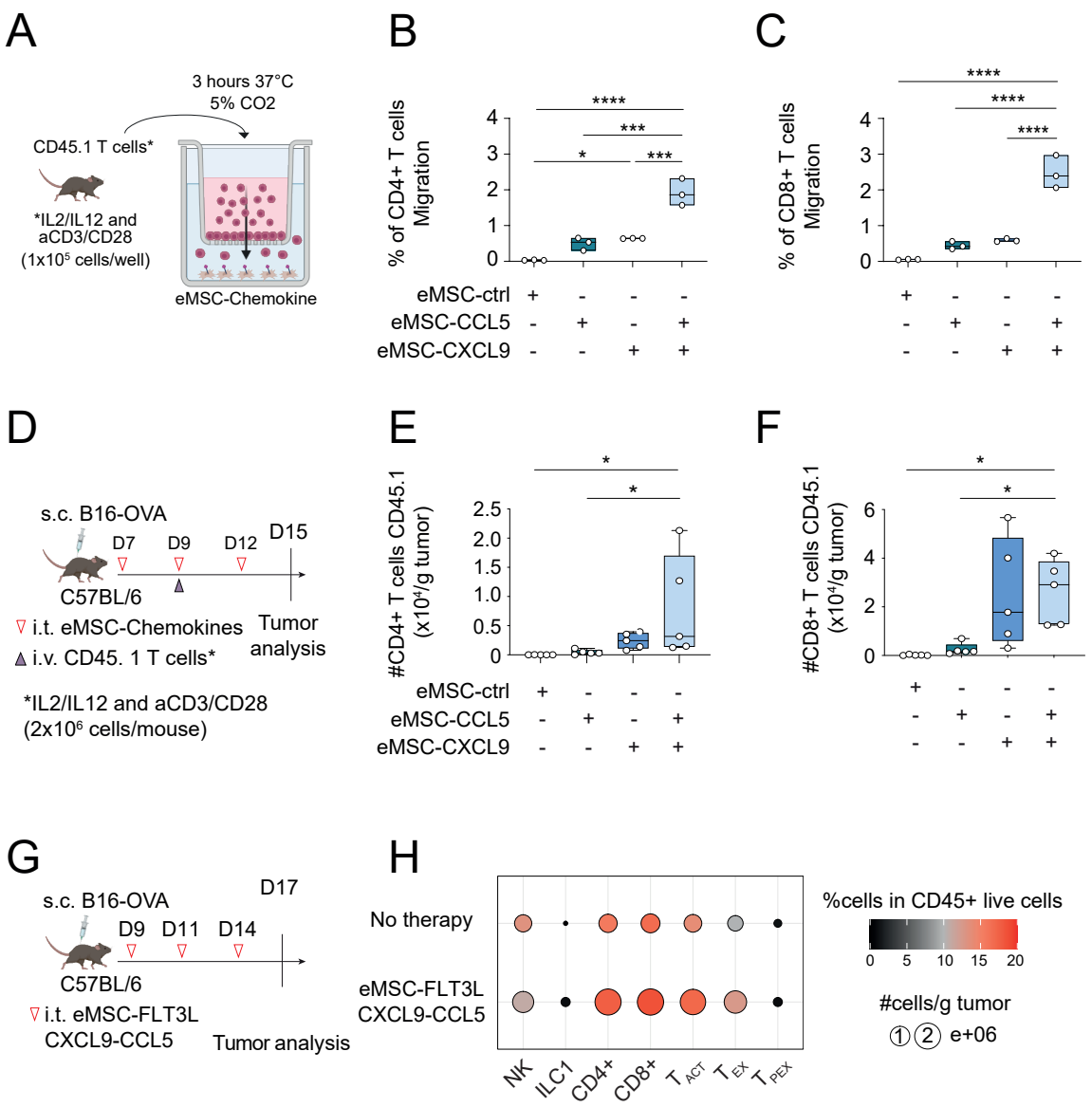

618

619 **<u>Figure 7:</u> Intra-tumoral delivery of eMSC co-expressing FLT3L, CXCL9 and CCL5**
620 **stimulates the infiltration of activated $CD4^+$ and $CD8^+$ T cells.**
621 **(A**) Experimental scheme of the migration assay. eMSC-CXCL9, eMSC-CCL5 and eMSC-Ctrl
622 were plated in the lower compartment of Boyden chambers, 24 hours before the migration
623 assay. *Ex-vivo* polarized CD45.1 T cells were then transferred to the upper compartment of the
624 culture system and incubated at 37°C for 3 h.
625 **(B-C)** Quantification of the migration index of CD4+ (B) and CD8+ (C) T cells. The migration
626 index was obtained by counting the number of T cells that migrated to the bottom chambers,
627 regarding the number of T cells initially put on top of the chambers. (n=3, one experiment, *p
628 < 0.05, ***p < 0.001, ****p < 0.0001, one-way ANOVA test with Tukey's multiple
629 comparisons).
630 **(D)** Experimental design for adoptive Th1-CD45.1 T cells transfer in B16-OVA-bearing mice.
631 CD45.2 WT mice were injected subcutaneously (s.c.) with B16-OVA on day 0. At day 7, 9 and
632 12, mice were injected into the tumor (i.t.) with eMSC-CCL5, eMSC-CXCL9 or eMSC-Ctrl.
633 At day 9, mice were injected intra-venously (i.v.) with Th1-CD45.1 T cells, previously activated
634 and polarized *ex vivo*. Tumors were harvested at day 15 and analyzed by flow cytometry.
635 **(E-F)** Quantification of the absolute number of CD45.1 $CD4^+$ T cells/g tumor (E) and CD45.1
636 $CD8^+$ T cells/g tumor (F). (n=5 mice per group, one experiment, *p < 0.05, one-way ANOVA
637 test with Dunnett's multiple comparisons).
638 **(G)** Experimental design to assess the infiltration of DC1s in the tumors after injection of
639 eMSC-FLT3L-CCL5-CXCL9. C57BL/6 mice were injected subcutaneously with B16-OVA
640 tumors on day 0. At day 9, 11 and 14, mice were injected into the tumor (i.t.) with eMSC-
641 FLT3L-CXCL9-CCL5. Tumors were harvested at day 17 and analyzed by flow cytometry.
642 **(H)** Quantification of the absolute number and the frequencies in $CD45^+$ live cells of NK, ILC1,
643 $CD4^+$, $CD8^+CD44^+$ activated (T_{ACT}), $CD8^+CD44^+PD1^+Tim3^-$ progenitor exhausted (T_{PEX}) and
644 $CD8^+CD44^+PD1^+Tim3^+$ exhausted (T_{EX}) T cells. Dots represent the absolute number of cells/g
645 tumor while the colours represent the frequencies of cells in $CD45^+$ live cells.

646 **Intra-tumoral delivery of eMSC co-expressing FLT3L, CXCL9 and CCL5 recapitulates**
647 **anti-tumor immunity**
648 Having shown that eMSC-FLT3L-CXCL9-CCL5 immunotherapy had an impact on the
649 infiltration of immune cells in the tumors, we wondered if it would also confer anti-tumor
650 immunity. To test this, we did three injections of eMSC-FLT3L-CXCL9-CCL5 in B16-OVA
651 tumors (Fig. **8A**). We observed a significant reduction in tumor growth (Fig. **8B**), tumor size
652 (Fig. **8C**) and tumor weight (Fig. **8D**) at a late time point.
653 Finally, we wanted to assess if eMSC-FLT3L-CXCL9-CCL5 immunotherapy would also
654 overcome resistance to ICB, by treating the mice with or without aPD1/aCTLA-4
655 immunotherapy (Fig. **8E**). We found that even if ICB alone reduced the tumor growth (Fig. **8F**)
656 and expand the survival of mice (Fig. **8G**), the synergy of both eMSC-FLT3L-CXCL9-CCL5
657 and ICB was needed to eradicate the tumor in a fraction of treated mice (Fig. **8G**).
658 Altogether, these data indicate that eMSC-FLT3L-CXCL9-CCL5 immunotherapy activates
659 anti-tumor immunity and partially overcome resistance to ICB.

Fig8. Intra-tumoral delivery of eMSC co-expressing FLT3L, CXCL9 and CCL5 is sufficient to activate anti-tumor immunity

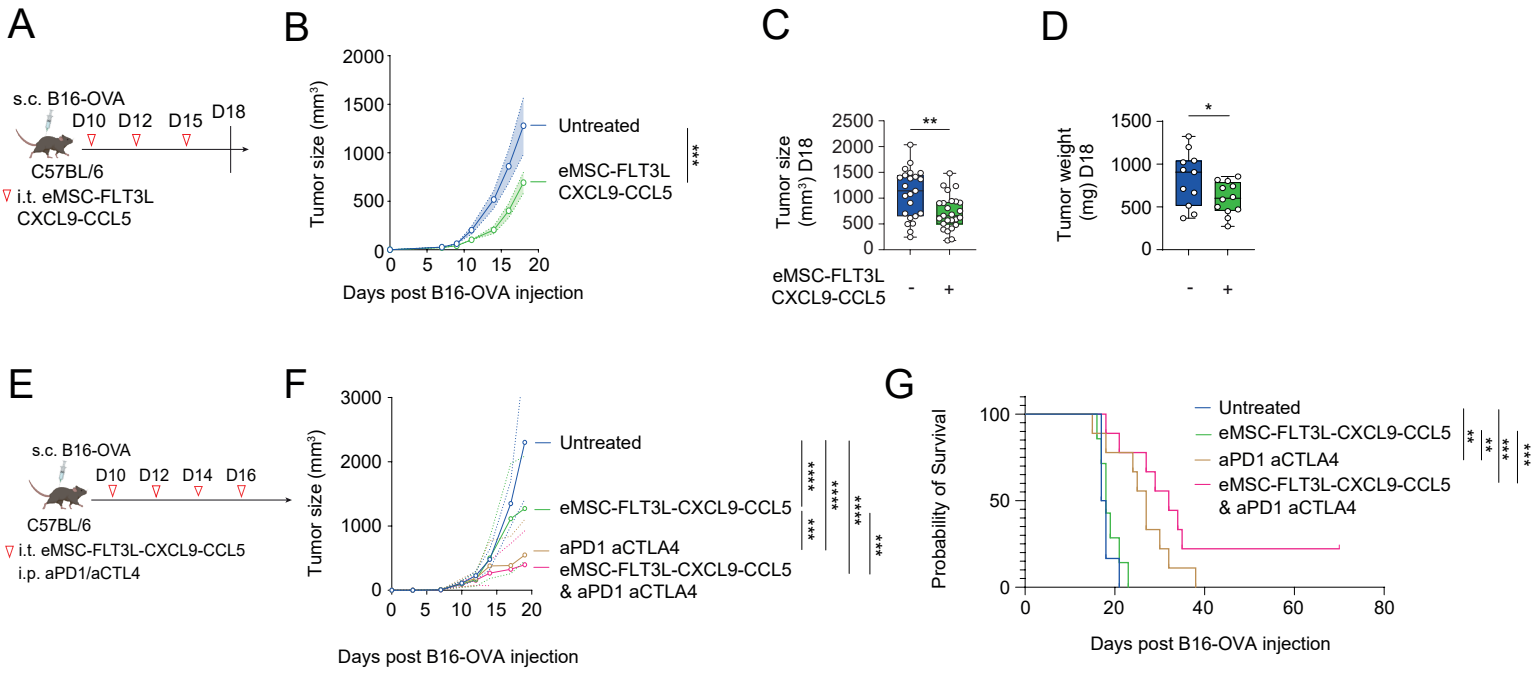

660

<u>Figure 8:</u> Intra-tumoral delivery of eMSC co-expressing FLT3L, CXCL9 and CCL5 is sufficient to activate anti-tumor immunity

(A) Experimental design to assess the anti-tumor effect of eMSC-FLT3L-CCL5-CXCL9. C57BL/6 mice were injected subcutaneously with B16-OVA tumors on day 0. At day 10, 12 and 15 mice were injected into the tumor (i.t.) with eMSC-FLT3L-CXCL9-CCL5. Tumors were harvested at day 18.

(B) Tumor growth curves. A line represents the mean and SD is shown with the colored area. (n=5, representative of 4 independent experiments, ***$p < 0.001$, two-way ANOVA-test with Šídák's multiple comparisons).

(C) Tumor size at day 18. (n=23-24, four independent experiments, **$p < 0.01$, two-tailed unpaired t-test).

(D) Tumor weight at day 18. (n=11-12, two independent experiments, *$p < 0.05$, two-tailed unpaired t-test).

(E) Experimental design to evaluate the response of tumors treated with eMSC-FLT3L-CXCL9-CCL5, together with immune checkpoint blockade. Mice were injected subcutaneously (s.c.) with B16-OVA on day 0. At day 10, 12, 14 and 16, mice were injected into the tumor (i.t.) with eMSC-FLT3L-CXCL9-CCL5 and intraperitoneally with immune checkpoint blockade (anti-PD-1 and anti-CTLA-4).

(F) Tumor growth curves. (A line represents the mean and SD is shown with the colored doted lines, n=6-8 mice per group, one experiment, ***$p < 0.001$, ****$p < 0.0001$, two-way ANOVA-test with Tukey's multiple comparisons).

(Q) Survival curves. (n=6-8 mice per group, one experiment, log-rank (Mantel-Cox) test)

683 **DISCUSSION**
684

685 Here, we identify a novel immunotherapeutic platform defined by the engraftment of *ex*
686 *vivo* engineered, autologous mesenchymal stromal cells (eMSCs) within primary tumors. In
687 line with previous studies (*14*), we observe a therapeutic synergy between FLT3L and the
688 poly(I:C) adjuvant. We show that this anti-tumor response relies on DC1s, T and NK cells.
689 Interestingly, eMSC-FLT3L and poly(I:C) did not expand Tregs in the tumor. Altogether, we
690 show that engineered stromal cells provide a novel avenue to deliver FLT3L specifically at the
691 tumor site.

692 We next evidence that poly(I:C) up-regulates multiple chemokines within the TME,
693 namely CXCL9 and CCL5, which are ligands for CXCR3 and CCR5 respectively.
694 Pharmacological experiments demonstrate that CXCR3 and CCR5 control intra-tumoral DC1s
695 accrual. Furthermore, we show that CXCL9 and CCL5 delivery with FLT3L is sufficient to
696 recapitulate pre-DC1s infiltration and DC1s expansion within tumors. CXCR3 and CCR5 are
697 found on activated T and NK cells but also on circulating DC precursors (*42*) (*43*) (*44*). We
698 found that T cells and NK cells are dispensable for the aegis of CXCL9 and CCL5 on DCs
699 recruitment. Intra-tumoral ligands for CXCR3 and CCR5 might originate from multiple sources
700 including DC1s themselves (*5*) (*6*) (*43*) (*44*), what may contribute to the maintenance of a
701 positive feedback loop supporting the maintenance of intra-tumoral DC1s.

702 Finally, we show that eMSC-FLT3L-CCL5-CXCL9 achieve the local recruitment of
703 human DC1s in the dermis of BRGSF immunodeficient mice reconstituted with human $CD34^+$
704 HSCs (*45*). However, the nature of the responding circulating progenitors remains to be
705 identified since multiple cellular populations had been proposed to act as equivalent of murine
706 pre-DCs in the human system (*31*, *47*, *48*)

707 In line with previous studies (*43*),(*44*), we demonstrate that injection of eMSC-FLT3L-
708 CXCL9-CCL5 increase T and NK/ILCs cells infiltration within tumors. Therefore, local
709 delivery of chemokines might achieve a double effect on pre-DCs infiltration and local effectors
710 recruitment. However, it remains unclear whether the recruitment of activated T and NK cells
711 is a direct consequence of chemokines signalling or an indirect effect mediated by the migration
712 of activated dendritic cells to the tumor-draining lymph node.

713 We have found that CXCL9 and CCL5 in addition to FLT3L stimulates the expression
714 of maturation markers like CD40 on intra-tumoral DCs. Further experiments could address if
715 lymphocytes recruited by CXCL9 or CCL5 might engage DCs and activate their maturation,
716 possibly via CD40 signalling.

717 Lastly, when combining eMSC-FLT3L-CXCL9-CCL5 to aPD1/aCTLA-4
718 immunotherapy, we manage to partially overcome primary resistance to immune checkpoint
719 blockade. It will be interesting to decipher if and how eMSC-FLT3L-CXCL9-CCL5 reshape
720 broadly the immune infiltration with possible roles of CXCL9+ macrophages (*49*), stem
721 immunity hubs (J. H. Chen et al. 2024) or TLS (*9*).
722 Altogether, our results support the idea that intra-tumoral delivery of eMSC-FLT3L
723 together with CXCR3- and CCR5-ligands is efficient to reprogram immune infiltration in the
724 TME. As claimed by Bae et al.(*50*), we believe that autologous mesenchymal stromal cells
725 represent a promising platform to locally deliver bioactive factors and achieve their sustained
726 production at the target site. Furthermore, this approach might also mitigate systemic toxicity
727 to optimize immunotherapy outcomes Lastly, our findings provide strong rationale for further
728 translational development.

729 **MATERIALS AND METHODS**
730

731 **Study Design**
732 The aim of this study was to develop a local DC-targeted immunotherapy purposed to stimulate
733 DCs infiltration and expansion within solid tumors. To that end, we injected engineered
734 autologous mesenchymal stromal cells within B16-OVA melanoma tumors and assessed the
735 anti-tumor immunity, DCs and T cells infiltration. Specific role of immune cells was assessed
736 with genetically modified mouse strains or depleting antibodies. We also evaluated the effect
737 of our therapies on the immune cells of the tdLN. Lastly, we tested if our immunotherapy was
738 transferrable to human settings by using BRGSF HIS mice. Most of the results in this study is
739 flow cytometry analysis and tumor follow-up. Experiments in this study were performed
740 between one and two times, unless otherwise stated in the figure captions.
741

742 **Mice**
743 Mice were housed at the INSERM U1149 CRI, Medicine school site Bichat or at the Paris
744 Institut Pasteur animal house facilities. Wild type C57BL/6J and CD45.1 mice were purchased
745 from Janvier and kept in our facility. IRF8-GFP (B6.Cg-Irf8tm2.1Hm/J), *XCR1*^{cre}, ROSA26-
746 LSL-RFP (Gt(ROSA)26Sortm1Hjf) and ROSA26-LSL-DTA (B6.129P2
747 Gt(ROSA)26Sortm1(DTA)Lky/J)(*51*) mice were kindly provided by Dr. Marc Dalod (Center
748 of Immunology Marseille-Luminy, Marseille). XCR1^{DTA} and XCR1^{RFP} mice were generated as
749 described(*37*). OT-I *RAG2*$^{-/-}$ CD45.1 mice were kindly provided by Dr. Sébastian Amigorena
750 (Curie institute, Paris). BALB/c Rag2$^{-/-}$ IL2rγ$^{-/-}$ Sirpα^{NOD} (BRGS), BALB/c Rag2$^{-/-}$ IL2rγ$^{-/-}$
751 Sirpα^{NOD} Flt3$^{-/-}$ (BRGSF) mice and BRGSF-HIS mice were provided by the Human Disease
752 model Core facility (Institut Pasteur, Paris). The study was approved by the local ethics
753 committee (Comité d'éthique Paris Nord n°121 or CEEA89) and the French Ministry of
754 Education and Research under the authorization number APAFIS#15373 and APAFIS #48865.
755 Animal care and treatment were conducted with national and international laws and policies
756 (European Economic Community Council Directive 86/609; OJL 358; December 12, 1987).
757 All experiments were performed in accordance with the Federation of European Laboratory
758 Animal Science Association (FELASA) guidelines, institutional guidelines and the French law.
759

760 **BRGSF humanized immune system mice (BRGSF-HIS)**
761 Briefly, cord blood CD34^{+} cells (CRB de la Banque de Sang de Cordon, AP-HP, Paris) were
762 isolated with affinity matrices according to the manufacturer's instructions (Miltenyi Biotec)

763 and subsequently phenotyped for CD34 and CD38 expression. Newborn (5–9 days old) pups
764 received sublethal irradiation (3 Gy) and were injected intra-hepatically with 3×10^5
765 $CD34^+$ human cord blood cells. 12 and 16 weeks after graft, reconstitution of the human
766 immune system was confirmed by analysis of human CD45, CD19, CD3, CD4, CD8 expression
767 on live leukocytes in the blood using flow cytometry. All animal studies were approved by the
768 Pasteur Institute Safety Committee in accordance with French and European Guidelines
769 (Committee for Ethics in Animal Experimentation 240006) and validated by the French
770 Ministry of Education and Research (APAFIS #49211-2024042612197924 v3).
771

772 **Tumor cell lines**
773 B16-OVA and YUM-OVA cell lines were generated by lentiviral transduction. B16F10, B16-
774 FLT3L(*52*) and B16-OVA cell lines were cultured in RPMI Medium 1640 (Gibco®)
775 supplemented with GlutaMAX, 10% heat-inactivated fetal bovine serum (FBS) (Gibco®),
776 50µM β-mercaptoethanol (ThermoFisher) and 100U/mL penicillin-streptomycin
777 (ThermoFisher). YUM-OVA cell lines were cultured in DMEM (Gibco®) supplemented with
778 GlutaMAX, 10% heat-inactivated FBS (Gibco®), 50µM β-mercaptoethanol (ThermoFisher)
779 and 100U/mL penicillin-streptomycin (ThermoFisher). Cells were maintained at 37°C and 5%
780 CO_2.
781

782 **Tumor models**
783 For the grafted tumor model, tumor cells were harvested during the exponential growth phase
784 using 0.05% Trypsin-EDTA (Gibco), washed twice in PBS, and counted using trypan blue
785 exclusion. Mice were subcutaneously inoculated with 5×10^5 to 1×10^6 tumor cells suspended in
786 100µL of un-supplemented RPMI medium. Tumor dimensions were recorded three times per
787 week using a digital caliper, and tumor volume (V) was calculated using the formula
788 $V=(L\times W\times W)/2$, with volume expressed in mm^3. Mice were monitored daily, and endpoints
789 were established based on signs of distress, including pain, lethargy, dehydration, ulceration,
790 or tumor necrosis. Mice were sacrificed when these criteria were met or when tumor volume
791 reached between 1500 and 2000 mm^3 to generate survival curves.

792 **Generation of engineered mesenchymal stromal cells**
793

794 **Generation of mesenchymal stromal cells**

795 Mesenchymal stromal cells (MSC) were generated from mouse embryonic fibroblasts (MEFs)
796 from individual C57/BL6 embryos at embryonic day 13 and were kindly provided by Dr.
797 Loredana Saveanu. Practically, the embryo body was digested with 0.05% trypsin and 0.02%
798 EDTA in Hanks balanced salt solution at 37°C for 30 minutes. The single cell suspension
799 obtained after digestion was resuspended in high glucose DMEM medium containing 10% FCS,
800 2mM L-glutamine, 100U/ml penicillin and 100µg/ml streptomycin and seeded on 0.1% gelatin
801 (Sigma G1890) coated tissue culture dishes at $5x10^4$ cells/cm^2. Cells growing on the gelatin-
802 coated dishes were harvested and cell passages were repeated in DMEM medium containing
803 10% FCS, 2mM L-glutamine, 100U/ml penicillin and 100µg/ml streptomycin. Immortalized
804 cells were obtained at passage 20.
805

806 **Generation of adipose-derived mesenchymal stromal cells**

807 Method was adapted form Dr. Geneviève Marcelin. Inguinal and visceral fat of C57BL/6 mice
808 were cut in small pieces and digested with 6 to 8mL of digestion mix, containing high glucose
809 DMEM (ThermoFisher), 1mg/mL collagenase A (Roche) resuspended in HBSS
810 (ThermoFisher), 100U/mL HEPES (ThermoFisher), 100U/mL penicillin/streptomycin
811 (ThermoFisher) and 1mg/mL BSA. After 40min digestion at 37°C, the digestion was
812 mechanically ended with a syringe and a needle of 18G. Cell suspension was then filtered on a
813 100µm cell strainer and centrifuged. Floating adipocytes and red blood cells (ACK lysis,
814 ThermoFisher) were removed. Cells were enriched in CD45-Ter119- cells using a StemCell
815 Magnet and biotin anti-CD45 and anti-Ter119 antibodies. Enriched cells were then cultured in
816 an adherent flask with DMEM (Gibco®) supplemented with GlutaMAX, 20% heat-inactivated
817 FBS (Gibco®), 50µM β-mercaptoethanol (ThermoFisher) and 100U/mL penicillin-
818 streptomycin (ThermoFisher). Cells were maintained at 37°C and 5% CO_2.
819

820 **Engineering of mesenchymal stromal cells**

821 Human FLT3L, CXCL9 and CCL5 were amplified by PCR from previously obtained or
822 commercial cDNA (Horizon Discovery) and cloned into pMX retroviral vectors (detailed in the
823 Supplementary Table 1). To generate viral particles, the Platinum-E (Plat-E) Retroviral
824 Packaging Cell Line (kindly provided by Laurie Menger) was transfected with 1,2µg plasmid,
825 CaCl2 and BBS. MSCs were then transduced with the viral supernatant and 8µg/mL polybrene.

826 Transduced MSCs were selected using 2µg/mL puromycin (ThermoFisher) and sorted on their
827 expression of membrane-bound FLT3L (antibody details provided in the Supplementary Table
828 1) and/or their expression of eGFP or mCherry reporters. Engineered MSCs were cultured in
829 DMEM (Gibco®) supplemented with GlutaMAX, 10% heat-inactivated FBS (Gibco®), 50µM
830 β-mercaptoethanol (ThermoFisher), 2µg/mL puromycin (ThermoFisher) and 100U/mL
831 penicillin-streptomycin (ThermoFisher), under standard culture conditions of 37°C and 5%
832 CO_2.
833
834 ***In vitro* experiments**
835
836 **T cells isolation, activation and polarization**
837 $CD4^+$ and $CD8^+$ T cells were isolated from the draining lymph nodes and spleens of 10- to 12-
838 week-old CD45.1 mice. Purification was performed using negative selection with a biotin-
839 conjugated antibody cocktail, followed by anti-biotin magnetic beads and separation with a
840 MACS MultiStand separator. For *in vitro* stimulation, purified T cells were cultured on plates
841 coated with anti-CD3 (2µg/mL; clone 17A2) and anti-CD28 (2µg/mL; clone 3751; BioLegend)
842 in the presence of recombinant IL-2 (5µg/mL; BioLegend). To promote Th1 differentiation,
843 cultures were supplemented with recombinant IL-12 (10ng/mL; BioLegend) and anti-IL-4
844 (5µg/mL; clone MP4-25D2; BioLegend).
845
846 **Migration assay**
847 Cell migration assays were conducted using 24-well transwells inserts with 5-µm pore
848 polycarbonate membranes (Corning, catalog #CLS3421). Engineered mesenchymal stromal
849 cells (eMSCs) expressing CCL5 or CXCL9 were seeded at a density of 250,000 cells per well
850 in the lower chamber. Once the eMSCs reached confluency, the culture medium was replaced
851 with serum-free DMEM. A total of 100,000 CD45.1 Th1-polarized T cells were resuspended
852 in serum-free DMEM, and 100µL of the cell suspension was carefully added to the upper
853 chamber of the Transwell insert. The upper chamber was then gently placed into the lower
854 chamber using sterile forceps, ensuring proper immersion in the culture medium. The plate was
855 incubated at 37°C for 3 hours. Following incubation, the supernatant was collected to quantify
856 T-cell migration by flow cytometry.
857
858

859 ***In vivo* experiments**
860

861 **HSPCs differentiation in membrane extract plugs**

862 Immunomagnetic negative selection was used to isolate mouse stem and progenitor cells
863 (HSPC) from CD45.1 mice using the EasySep™ Mouse Hematopoietic Progenitor Cell
864 Isolation Kit, following the manufacturer's instructions. A total of 10^4 hematopoietic stem and
865 progenitor cells (HSPCs) per plug were subcutaneously injected alongside engineered
866 mesenchymal stromal cells (eMSCs) at a 1:50 ratio (HSPC/eMSC) in 200 µL of ice-cold
867 Matrigel® (Thermo Fisher). Mice were euthanized on day 12 of differentiation via cervical
868 dislocation, and Matrigel® plugs were excised for further analysis. The plugs were sectioned
869 and enzymatically digested in HBSS (Life Technologies) containing 1% FBS, 0.37U/mL
870 Collagenase D (Roche), 10µg/mL DNase I (Roche), and 1mg/mL Dispase (Sigma-Aldrich) at
871 37°C for 30 minutes. Following digestion, the tissue was smashed on a 100-µm strainer
872 (Corning), and the resulting cell suspension was collected and resuspended in FACS buffer for
873 flow cytometry analysis. For experiments involving recombinant FLT3L, human FLT3Lwas
874 used at a concentration of 100ng/mL.
875

876 ***In Vivo* Treatment with Engineered Stromal Cells**

877 Intra-tumoral injections of eMSCs started when the tumors were between 50 and $100mm^3$. Mice
878 were treated with 5×10^5 to 1×10^6 eMSC-FLT3L, in combination with 25µg/mouse of poly I:C
879 LMW (InVivoGen). We designed our intra-tumoral cell-based therapy as two injections of
880 eMSC-FLT3L (day 7 and day 12) and one injection of poly(I:C) (day 9). Mice that were later
881 treated with 5×10^5 to 1×10^6 eMSC-FLT3L-CXCL9-CCL5 received three injections of eMSCs.
882 In the latest experiments, mice developed tumors with the desired injectable size few days later
883 than the initial schedule. Thus, the start of injections was postponed but the number and
884 frequencies of injections was kept.
885

886 **Immune Checkpoint Blockade (ICB) Treatment**

887 Mice received intraperitoneal (i.p.) injections of 200µg anti-PD-1 (clone RMP1-14, BioXcell)
888 and 200µg of anti-CTLA-4 (clone 9H10, BioXCell). An isotype antibody (clone 1-113,
889 BioXCell) and IgG control (clone MPC11, BioXCell) was used as a control. All antibodies
890 were administered intra-peritoneally at treatment initiation and subsequently every two days
891 until reaching 5 injections.
892

893 **CD4, CD8 and NK cells depletion**

894 For the depletion of $CD4^+$ T cells, $CD8^+$ T cells, and $NK1.1^+$ cells, mice were treated with 200µg
895 of anti-CD4 (clone GK1.5, BioXCell BE0003-1), 200µg of anti-CD8 (clone 2.43, BioXCell
896 BE0061), and 200µg of anti-NK1.1 (clone PK136, BioXCell BE0036). As controls, 300µg of
897 IgG2a isotype (clone C1.18.4, BioXCell BE0085) and 500µg of rat IgG2b isotype (clone LFT-
898 2, BioXCell BE0090) were used. All antibodies were administered intraperitoneally at the
899 initiation of treatment and subsequently every three days, until reaching 4 injections.
900

901 **CXCR3- and CCR5-antagonists' treatments**

902 Mice received intraperitoneal injections of either maraviroc (30mg/kg, 500µg/mouse), a CCR5
903 antagonist, or AMG 487 (200µg/mouse), a CXCR3 antagonist. Both agents were dissolved in
904 a vehicle of dimethyl sulfoxide (DMSO). Administration started at the initiation of treatment
905 and continued every two days until day 15, where samples were collected for flow cytometry
906 analysis.
907

908 **SIINFEKL re-challenging in survivor mice**

909 Tumor-eradicated mice underwent *in vivo* restimulation via subcutaneous injection of 1µg OVA
910 257-264 peptide (SIINFEKL; Sigma-Aldrich) dissolved in 100µl phosphate-buffered saline
911 (PBS). The injection site was located in the dorsal flank region. Three days post-restimulation,
912 mice were euthanized, and inguinal draining lymph nodes were excised for subsequent analysis.
913

914 **Adoptive T cell transfer**

915 $1x10^5$ eMSCs were injected in B16-OVA tumors at day 7, 9 and 12. At day 9, $2x10^6$ Th1-
916 polarized CD45.1 T cells (previously described) were intravenously administered.
917

918 **Synthetic niches (plugs)**

919 $1x10^6$ eMSC-Ctrl or eMSC-FLT3L-CXCL9-CCL5 were injected subcutaneously (s.c.) in
920 200µL solution, containing 150µL of Geltrex LDEV-Free Reduced Growth Factor Basement
921 Membrane Matrix and 50µL of PBS. The synthetic niches (plugs) were harvested and analyzed
922 by flow cytometry 10 days after the injection.

923 **Mouse tissues processing**
924 Murine tumors, tumor-draining lymph nodes (LNs), spleens, or synthetic niches were harvested
925 and subjected to enzymatic digestion. Tissues were incubated in 3mL of digestion buffer,
926 comprising Hank's Balanced Salt Solution (HBSS) supplemented with calcium and magnesium
927 (Thermo Fisher), 75µg/mL Collagenase D (Roche), and 0.02mg/mL DNase I (Thermo Fisher),
928 at 37°C for 30 minutes. Single-cell suspensions were then generated by smashing the digested
929 tissues through 70µm cell strainers (Corning). Spleen red blood cells were lysed using ACK
930 lysis buffer (ThermoFisher). The absolute number of live immune cells in each tissue cell
931 suspension was assessed using AccuCheck Counting Beads (ThermoFisher) along with anti-
932 CD45 and DAPI stainings on BD LSR-Fortessa X20 or BD Symphony A5 (BD Biosciences).
933
934 **Flow cytometry analysis and fluorescent-activated cell sorting**
935 After tissue processing and cell counting, Fc-receptor were blocked using FcBlock for 20min
936 at 4°C. Viability was assessed using 7-AAD (Biolegend), Zombie dyes (BioLegend), or
937 Live/dead fixable stains (ThermoFisher). Extracellular staining was performed in FACS buffer
938 (PBS (Life Technologies), 3% FBS (ThermoFisher), and 2 mM EDTA (Life Technologies))
939 during 30min at 4°C. Labelling with $H2K^b$-SIINFEKL tetramers (MBL) was performed at room
940 temperature for 30min. For intra-cellular stainings, single cell suspensions were then fixed
941 during 30min and stained during 30min using a fixation/permeabilization kit (eBiosciences,
942 transcription factor staining buffer). For intra-cellular IFNγ staining, single-cell suspensions
943 were first restimulated *ex vivo* with 2µM OVA257–264 peptide (SIINFEKL, GenScript) for 5
944 hours at 37°C in 5% CO2, followed by a 4-hour incubation with 5µg/mL Brefeldin A (Sigma
945 Aldrich). Cells were subsequently labelled with surface antibodies, fixed with 4%
946 paraformaldehyde (PFA; Thermo Fisher), permeabilized with a solution of 1% BSA, 0.1%
947 saponin, and 0.02% sodium azide in PBS, and stained with an intracellular cytokine staining
948 (ICS) antibody panel. A comprehensive list of antibodies used is provided in Supplementary
949 Table 1. Flow cytometry data were acquired using BD LSR-Fortessa X20, BD Symphony A5
950 (BD Biosciences) or ID7000 Spectral (Sony). Cells sorting was performed using a BD
951 FACSMelody™ Cell Sorter equipped with BD FACSDiva software. Data were analyzed with
952 FlowJo software.
953
954 **Multiplex chemokines analysis**
955 Dissected tumor samples were weighted and homogenized in 1mL of 1x phosphate-buffered
956 saline (PBS) supplemented with protease inhibitor, using a Fisherbrand™ 150 handheld
957 homogenizer. Homogenates were then centrifuged at 14,000 x *g* for 15 minutes, and the

958 resulting supernatants were collected. The concentrations of pro-inflammatory chemokines
959 within the supernatants were quantified using the LEGENDplex™ MU Proinflammatory
960 Chemokine Panel 1 and 2 (BioLegend), following the manufacturer's instructions. Samples
961 were analyzed by flow cytometry on a BD FACS LSRFortessa. Data were analyzed using
962 LEGENDplex™ software (BioLegend). Chemokine concentrations were normalized to total
963 protein concentration, which was estimated using the initial tumor mass.
964

965 **Immunofluorescence**

966 Protocol was adapted from Laforêts et al. (*53*). Tumors were harvested and embedded in 5%
967 agarose. 350µm thick slices of non-fixed fresh samples were obtained using a vibratome
968 (LEICA, VT1200S), with blade speed between 0.5 and 0.75 mm/s and the amplitude at 1mm.
969 Samples were then collected in phenol-red free DMEM medium, containing 10% FBS, 1%
970 penicillin/streptomycin and 4mM L-glutamine. Live tumor samples were then put in a 35mm
971 glass bottom dish, filled with the before mentioned medium. Images were taken with a Nikon
972 Ti2E, equipped with a 20X objective, a spinning disk and a temperature-controlled chamber at
973 37°C. Images were analyzed with Fiji software.
974

975 **Statistical Analysis**

976 Statistical analysis was performed using Prism 10 (GraphPad Software Inc., USA). Statistical
977 analysis and verification of normal distribution were performed using GraphPad Prism
978 software. For comparisons of two groups, two-tailed paired or unpaired Student's *t* test was
979 used. When three or more groups were compared, a one-way or two-way analysis of variance
980 (ANOVA) test was used. Precise tests are described in the figure legends. A p-value of less
981 than 0.05 was considered as significant. The number of biological as well as experimental
982 replicates is indicated in figure legend. Data are presented as means ± SD, means ± SEM,
983 median ± quartile, or violin plots as described in the figure legends. In all figures, $*P < 0.05$,
984 $**P < 0.01$, and $***P < 0.001$; ns, not significant.
985

986 **Supplementary Materials**

987 Fig. S1 to S5

988 Table S1

References and Notes

1. M. J. Pittet, M. Di Pilato, C. Garris, T. R. Mempel, Dendritic cells as shepherds of T cell immunity in cancer. *Immunity* **56**, 2218–2230 (2023).

2. D. S. Chen, I. Mellman, Oncology meets immunology: the cancer-immunity cycle. *Immunity* **39**, 1–10 (2013).

3. V. Bosteels, S. Janssens, Striking a balance: new perspectives on homeostatic dendritic cell maturation. *Nat Rev Immunol*, doi: 10.1038/s41577-024-01079-5 (2024).

4. M. T. Chow, A. J. Ozga, R. L. Servis, D. T. Frederick, J. A. Lo, D. E. Fisher, G. J. Freeman, G. M. Boland, A. D. Luster, Intratumoral Activity of the CXCR3 Chemokine System Is Required for the Efficacy of Anti-PD-1 Therapy. *Immunity* **50**, 1498-1512.e5 (2019).

5. S. Spranger, D. Dai, B. Horton, T. F. Gajewski, Tumor-Residing Batf3 Dendritic Cells Are Required for Effector T Cell Trafficking and Adoptive T Cell Therapy. *Cancer Cell* **31**, 711-723.e4 (2017).

6. P. Meiser, M. A. Knolle, A. Hirschberger, G. P. de Almeida, F. Bayerl, S. Lacher, A.-M. Pedde, S. Flommersfeld, J. Hönninger, L. Stark, F. Stögbauer, M. Anton, M. Wirth, D. Wohlleber, K. Steiger, V. R. Buchholz, B. Wollenberg, C. E. Zielinski, R. Braren, D. Rueckert, P. A. Knolle, G. Kaissis, J. P. Böttcher, A distinct stimulatory cDC1 subpopulation amplifies CD8+ T cell responses in tumors for protective anti-cancer immunity. *Cancer Cell* **41**, 1498-1515.e10 (2023).

7. M. Di Pilato, R. Kfuri-Rubens, J. N. Pruessmann, A. J. Ozga, M. Messemaker, B. L. Cadilha, R. Sivakumar, C. Cianciaruso, R. D. Warner, F. Marangoni, E. Carrizosa, S. Lesch, J. Billingsley, D. Perez-Ramos, F. Zavala, E. Rheinbay, A. D. Luster, M. Y. Gerner, S. Kobold, M. J. Pittet, T. R. Mempel, CXCR6 positions cytotoxic T cells to receive critical survival signals in the tumor microenvironment. *Cell* **184**, 4512-4530 e22 (2021).

8. J. Duraiswamy, R. Turrini, A. Minasyan, D. Barras, I. Crespo, A. J. Grimm, J. Casado, R. Genolet, F. Benedetti, A. Wicky, K. Ioannidou, W. Castro, C. Neal, A. Moriot, S. Renaud-Tissot, V. Anstett, N. Fahr, J. L. Tanyi, M. A. Eiva, C. A. Jacobson, K. T. Montone, M. C. W. Westergaard, I. M. Svane, L. E. Kandalaft, M. Delorenzi, P. K. Sorger, A. Färkkilä, O. Michielin, V. Zoete, S. J. Carmona, P. G. Foukas, D. J. Powell, S. Rusakiewicz, M.-A. Doucey, D. Dangaj Laniti, G. Coukos, Myeloid antigen-presenting cell niches sustain antitumor T cells and license PD-1 blockade via CD28 costimulation. *Cancer Cell* **39**, 1623-1642.e20 (2021).

9. W. H. Fridman, M. Meylan, G. Pupier, A. Calvez, I. Hernandez, C. Sautès-Fridman, Tertiary lymphoid structures and B cells: An intratumoral immunity cycle. *Immunity* **56**, 2254–2269 (2023).

10. J. H. Chen, L. T. Nieman, M. Spurrell, V. Jorgji, L. Elmelech, P. Richieri, K. H. Xu, R. Madhu, M. Parikh, I. Zamora, A. Mehta, C. S. Nabel, S. S. Freeman, J. D. Pirl, C. Lu, C. B. Meador, J. L. Barth, M. Sakhi, A. L. Tang, S. Sarkizova, C. Price, N. F. Fernandez, G. Emanuel, J. He, K. Van Raay, J. W. Reeves, K. Yizhak, M. Hofree, A. Shih, M. Sade-Feldman, G. M. Boland, K. Pelka, M. J. Aryee, M. Mino-Kenudson, J. F. Gainor, I. Korsunsky, N. Hacohen, Human lung cancer harbors spatially organized stem-immunity hubs associated with response to immunotherapy. *Nat Immunol* **25**, 644–658 (2024).

1034 11. A. Magen, P. Hamon, N. Fiaschi, B. Y. Soong, M. D. Park, R. Mattiuz, E. Humblin, L.
1035 Troncoso, D. D'souza, T. Dawson, J. Kim, S. Hamel, M. Buckup, C. Chang, A.
1036 Tabachnikova, H. Schwartz, N. Malissen, Y. Lavin, A. Soares-Schanoski, B. Giotti, S.
1037 Hegde, G. Ioannou, E. Gonzalez-Kozlova, C. Hennequin, J. Le Berichel, Z. Zhao, S. C.
1038 Ward, I. Fiel, B. Kou, M. Dobosz, L. Li, C. Adler, M. Ni, Y. Wei, W. Wang, G. S. Atwal,
1039 K. Kundu, K. J. Cygan, A. M. Tsankov, A. Rahman, C. Price, N. Fernandez, J. He, N. T.
1040 Gupta, S. Kim-Schulze, S. Gnjatic, E. Kenigsberg, R. P. Deering, M. Schwartz, T. U.
1041 Marron, G. Thurston, A. O. Kamphorst, M. Merad, Intratumoral dendritic cell-CD4+ T
1042 helper cell niches enable CD8+ T cell differentiation following PD-1 blockade in
1043 hepatocellular carcinoma. *Nat Med* **29**, 1389–1399 (2023).

1044 12. K. Hildner, B. T. Edelson, W. E. Purtha, M. Diamond, H. Matsushita, M. Kohyama, B.
1045 Calderon, B. U. Schraml, E. R. Unanue, M. S. Diamond, R. D. Schreiber, T. L. Murphy,
1046 K. M. Murphy, Batf3 deficiency reveals a critical role for CD8alpha+ dendritic cells in
1047 cytotoxic T cell immunity. *Science* **322**, 1097–1100 (2008).

1048 13. A. R. Sánchez-Paulete, F. J. Cueto, M. Martínez-López, S. Labiano, A. Morales-
1049 Kastresana, M. E. Rodríguez-Ruiz, M. Jure-Kunkel, A. Azpilikueta, M. A. Aznar, J. I.
1050 Quetglas, D. Sancho, I. Melero, Cancer Immunotherapy with Immunomodulatory Anti-
1051 CD137 and Anti-PD-1 Monoclonal Antibodies Requires BATF3-Dependent Dendritic
1052 Cells. *Cancer Discov* **6**, 71–79 (2016).

1053 14. H. Salmon, J. Idoyaga, A. Rahman, M. Leboeuf, R. Remark, S. Jordan, M. Casanova-
1054 Acebes, M. Khudoynazarova, J. Agudo, N. Tung, S. Chakarov, C. Rivera, B. Hogstad,
1055 M. Bosenberg, D. Hashimoto, S. Gnjatic, N. Bhardwaj, A. K. Palucka, B. D. Brown, J.
1056 Brody, F. Ginhoux, M. Merad, Expansion and Activation of CD103(+) Dendritic Cell
1057 Progenitors at the Tumor Site Enhances Tumor Responses to Therapeutic PD-L1 and
1058 BRAF Inhibition. *Immunity* **44**, 924–938 (2016).

1059 15. K. C. Barry, J. Hsu, M. L. Broz, F. J. Cueto, M. Binnewies, A. J. Combes, A. E. Nelson,
1060 K. Loo, R. Kumar, M. D. Rosenblum, M. D. Alvarado, D. M. Wolf, D. Bogunovic, N.
1061 Bhardwaj, A. I. Daud, P. K. Ha, W. R. Ryan, J. L. Pollack, B. Samad, S. Asthana, V.
1062 Chan, M. F. Krummel, A natural killer-dendritic cell axis defines checkpoint therapy-
1063 responsive tumor microenvironments. *Nat Med* **24**, 1178–1191 (2018).

1064 16. S. Zelenay, A. G. van der Veen, J. P. Böttcher, K. J. Snelgrove, N. Rogers, S. E. Acton,
1065 P. Chakravarty, M. R. Girotti, R. Marais, S. A. Quezada, E. Sahai, C. Reis e Sousa,
1066 Cyclooxygenase-Dependent Tumor Growth through Evasion of Immunity. *Cell* **162**,
1067 1257–1270 (2015).

1068 17. J. M. Schenkel, R. H. Herbst, D. Canner, A. Li, M. Hillman, S.-L. Shanahan, G.
1069 Gibbons, O. C. Smith, J. Y. Kim, P. Westcott, W. L. Hwang, W. A. Freed-Pastor, G.
1070 Eng, M. S. Cuoco, P. Rogers, J. K. Park, M. L. Burger, O. Rozenblatt-Rosen, L. Cong,
1071 K. E. Pauken, A. Regev, T. Jacks, Conventional type I dendritic cells maintain a
1072 reservoir of proliferative tumor-antigen specific TCF-1+ CD8+ T cells in tumor-draining
1073 lymph nodes. *Immunity* **54**, 2338-2353.e6 (2021).

1074 18. M. L. Broz, M. Binnewies, B. Boldajipour, A. E. Nelson, J. L. Pollack, D. J. Erle, A.
1075 Barczak, M. D. Rosenblum, A. Daud, D. L. Barber, S. Amigorena, L. J. Van't Veer, A. I.
1076 Sperling, D. M. Wolf, M. F. Krummel, Dissecting the tumor myeloid compartment
1077 reveals rare activating antigen-presenting cells critical for T cell immunity. *Cancer Cell*
1078 **26**, 638–652 (2014).

1079 19. S. Hegde, V. E. Krisnawan, B. H. Herzog, C. Zuo, M. A. Breden, B. L. Knolhoff, G. D.
1080 Hogg, J. P. Tang, J. M. Baer, C. Mpoy, K. B. Lee, K. A. Alexander, B. E. Rogers, K. M.

1081 Murphy, W. G. Hawkins, R. C. Fields, C. J. DeSelm, J. K. Schwarz, D. G. DeNardo,
1082 Dendritic Cell Paucity Leads to Dysfunctional Immune Surveillance in Pancreatic
1083 Cancer. *Cancer Cell* **37**, 289-307.e9 (2020).

1084 20. S. Spranger, R. Bao, T. F. Gajewski, Melanoma-intrinsic β-catenin signalling prevents
1085 anti-tumour immunity. *Nature* **523**, 231–235 (2015).

1086 21. J. P. Böttcher, E. Bonavita, P. Chakravarty, H. Blees, M. Cabeza-Cabrerizo, S.
1087 Sammicheli, N. C. Rogers, E. Sahai, S. Zelenay, C. Reis e Sousa, NK Cells Stimulate
1088 Recruitment of cDC1 into the Tumor Microenvironment Promoting Cancer Immune
1089 Control. *Cell* **172**, 1022-1037.e14 (2018).

1090 22. M. Cabeza-Cabrerizo, C. M. Minutti, M. P. da Costa, A. Cardoso, R. P. Jenkins, J.
1091 Kulikauskaite, M. D. Buck, C. Piot, N. Rogers, S. Crotta, L. Whittaker, H. H. Encabo, J.
1092 W. McCauley, J. E. Allen, M. Pasparakis, A. Wack, E. Sahai, C. Reis e Sousa,
1093 Recruitment of dendritic cell progenitors to foci of influenza A virus infection sustains
1094 immunity. *Sci Immunol* **6**, eabi9331 (2021).

1095 23. C. Waskow, K. Liu, G. Darrasse-Jèze, P. Guermonprez, F. Ginhoux, M. Merad, T.
1096 Shengelia, K. Yao, M. Nussenzweig, The receptor tyrosine kinase Flt3 is required for
1097 dendritic cell development in peripheral lymphoid tissues. *Nat Immunol* **9**, 676–683
1098 (2008).

1099 24. H. J. McKenna, K. L. Stocking, R. E. Miller, K. Brasel, T. De Smedt, E. Maraskovsky, C.
1100 R. Maliszewski, D. H. Lynch, J. Smith, B. Pulendran, E. R. Roux, M. Teepe, S. D.
1101 Lyman, J. J. Peschon, Mice lacking flt3 ligand have deficient hematopoiesis affecting
1102 hematopoietic progenitor cells, dendritic cells, and natural killer cells. *Blood* **95**, 3489–
1103 3497 (2000).

1104 25. M. Momenilandi, R. Lévy, S. Sobrino, J. Li, C. Lagresle-Peyrou, H. Esmaeilzadeh, A.
1105 Fayand, C. Le Floc'h, A. Guérin, E. Della Mina, D. Shearer, O. M. Delmonte, A. Yatim,
1106 K. Mulder, M. Mancini, D. Rinchai, A. Denis, A.-L. Neehus, K. Balogh, S. Brendle, H.
1107 Rokni-Zadeh, M. Changi-Ashtiani, Y. Seeleuthner, C. Deswarte, B. Bessot, C.
1108 Cremades, M. Materna, A. Cederholm, M. Ogishi, Q. Philippot, O. Beganovic, M.
1109 Ackermann, M. Wuyts, T. Khan, S. Fouéré, F. Herms, J. Chanal, B. Palterer, J.
1110 Bruneau, T. J. Molina, S. Leclerc-Mercier, J.-L. Prétet, L. Youssefian, H. Vahidnezhad,
1111 N. Parvaneh, K. G. Claeys, R. Schrijvers, M. Luka, P. Pérot, J. Fourgeaud, C.
1112 Nourrisson, P. Poirier, E. Jouanguy, S. Boisson-Dupuis, J. Bustamante, L. D.
1113 Notarangelo, N. Christensen, N. Landegren, L. Abel, N. Marr, E. Six, D. Langlais, T.
1114 Waterboer, F. Ginhoux, C. S. Ma, S. G. Tangye, I. Meyts, N. Lachmann, J. Hu, M.
1115 Shahrooei, X. Bossuyt, J.-L. Casanova, V. Béziat, FLT3L governs the development of
1116 partially overlapping hematopoietic lineages in humans and mice. *Cell* **187**, 2817-
1117 2837.e31 (2024).

1118 26. M. Cabeza-Cabrerizo, J. van Blijswijk, S. Wienert, D. Heim, R. P. Jenkins, P.
1119 Chakravarty, N. Rogers, B. Frederico, S. Acton, E. Beerling, J. van Rheenen, H.
1120 Clevers, B. U. Schraml, M. Bajénoff, M. Gerner, R. N. Germain, E. Sahai, F. Klauschen,
1121 C. Reis e Sousa, Tissue clonality of dendritic cell subsets and emergency DCpoiesis
1122 revealed by multicolor fate mapping of DC progenitors. *Sci Immunol* **4**, eaaw1941
1123 (2019).

1124 27. P. Guermonprez, J. Helft, C. Claser, S. Deroubaix, H. Karanje, A. Gazumyan, G.
1125 Darasse-Jèze, S. B. Telerman, G. Breton, H. A. Schreiber, N. Frias-Staheli, E.
1126 Billerbeck, M. Dorner, C. M. Rice, A. Ploss, F. Klein, M. Swiecki, M. Colonna, A. O.
1127 Kamphorst, M. Meredith, R. Niec, C. Takacs, F. Mikhail, A. Hari, D. Bosque, T.

1128 Eisenreich, M. Merad, Y. Shi, F. Ginhoux, L. Rénia, B. C. Urban, M. C. Nussenzweig,
1129 Inflammatory Flt3l is essential to mobilize dendritic cells and for T cell responses during
1130 Plasmodium infection. *Nat Med* **19**, 730–738 (2013).

1131 28. V. N. Kapoor, S. Müller, S. Keerthivasan, M. Brown, C. Chalouni, E. E. Storm, A.
1132 Castiglioni, R. Lane, M. Nitschke, C. X. Dominguez, J. L. Astarita, A. T. Krishnamurty,
1133 C. B. Carbone, Y. Senbabaoglu, A. W. Wang, X. Wu, V. Cremasco, M. Roose-Girma, L.
1134 Tam, J. Doerr, M. Z. Chen, W. P. Lee, Z. Modrusan, Y. A. Yang, R. Bourgon, W.
1135 Sandoval, A. S. Shaw, F. J. de Sauvage, I. Mellman, C. Moussion, S. J. Turley, Gremlin
1136 1+ fibroblastic niche maintains dendritic cell homeostasis in lymphoid tissues. *Nat*
1137 *Immunol* **22**, 571–585 (2021).

1138 29. R. S. Lane, S. Z. Wu, C. Davidson, A. Byrne, B. D. Kayser, H. Huang, K. Williams, M.
1139 Fernandez, J. Jiang, J. Zhang, R. Asuncion, J. Decalf, M. Roose-Girma, W. P. Lee, L.
1140 McGinnis, S. Warming, W. Stephenson, S. Rost, C. Moussion, T. Biancalani, S. Müller,
1141 S. J. Turley, Fibroblastic FLT3L supports lymph node dendritic cells in the interfollicular
1142 niche. bioRxiv [Preprint] (2024). https://doi.org/10.1101/2024.08.12.607692.

1143 30. Y. Saito, C. S. Boddupalli, C. Borsotti, M. G. Manz, Dendritic cell homeostasis is
1144 maintained by nonhematopoietic and T-cell-produced Flt3-ligand in steady state and
1145 during immune responses. *Eur J Immunol* **43**, 1651–1658 (2013).

1146 31. J. Lee, G. Breton, T. Y. Oliveira, Y. J. Zhou, A. Aljoufi, S. Puhr, M. J. Cameron, R. P.
1147 Sekaly, M. C. Nussenzweig, K. Liu, Restricted dendritic cell and monocyte progenitors
1148 in human cord blood and bone marrow. *The Journal of experimental medicine*, doi:
1149 10.1084/jem.20141442 (2015).

1150 32. E. J. Clappaert, D. Kancheva, J. Brughmans, A. Debraekeleer, P. M. R. Bardet, Y.
1151 Elkrim, D. Lacroix, M. Živalj, A. E. I. Hamouda, J. A. Van Ginderachter, S.
1152 Deschoemaeker, D. Laoui, Flt3L therapy increases the abundance of Treg-promoting
1153 CCR7+ cDCs in preclinical cancer models. *Front Immunol* **14**, 1166180 (2023).

1154 33. G. Darrasse-Jèze, S. Deroubaix, H. Mouquet, G. D. Victora, T. Eisenreich, K. Yao, R. F.
1155 Masilamani, M. L. Dustin, A. Rudensky, K. Liu, M. C. Nussenzweig, Feedback control of
1156 regulatory T cell homeostasis by dendritic cells in vivo. *J Exp Med* **206**, 1853–1862
1157 (2009).

1158 34. L. K. Swee, N. Bosco, B. Malissen, R. Ceredig, A. Rolink, Expansion of peripheral
1159 naturally occurring T regulatory cells by Fms-like tyrosine kinase 3 ligand treatment.
1160 *Blood* **113**, 6277–6287 (2009).

1161 35. I. Melero, E. Castanon, M. Alvarez, S. Champiat, A. Marabelle, Intratumoural
1162 administration and tumour tissue targeting of cancer immunotherapies. *Nat Rev Clin*
1163 *Oncol* **18**, 558–576 (2021).

1164 36. G. Anselmi, K. Vaivode, C.-A. Dutertre, P. Bourdely, Y. Missolo-Koussou, E. Newell, O.
1165 Hickman, K. Wood, A. Saxena, J. Helft, F. Ginhoux, P. Guermonprez, Engineered
1166 niches support the development of human dendritic cells in humanized mice. *Nat*
1167 *Commun* **11**, 2054 (2020).

1168 37. R. Mattiuz, C. Wohn, S. Ghilas, M. Ambrosini, Y. O. Alexandre, C. Sanchez, A. Fries, T.
1169 P. Vu Manh, B. Malissen, M. Dalod, K. Crozat, Novel Cre-Expressing Mouse Strains
1170 Permitting to Selectively Track and Edit Type 1 Conventional Dendritic Cells Facilitate
1171 Disentangling Their Complexity in vivo. *Front Immunol* **9**, 2805 (2018).

1172 38. M. Sade-Feldman, K. Yizhak, S. L. Bjorgaard, J. P. Ray, C. G. de Boer, R. W. Jenkins,
1173 D. J. Lieb, J. H. Chen, D. T. Frederick, M. Barzily-Rokni, S. S. Freeman, A. Reuben, P.
1174 J. Hoover, A.-C. Villani, E. Ivanova, A. Portell, P. H. Lizotte, A. R. Aref, J.-P. Eliane, M.
1175 R. Hammond, H. Vitzthum, S. M. Blackmon, B. Li, V. Gopalakrishnan, S. M. Reddy, Z.
1176 A. Cooper, C. P. Paweletz, D. A. Barbie, A. Stemmer-Rachamimov, K. T. Flaherty, J. A.
1177 Wargo, G. M. Boland, R. J. Sullivan, G. Getz, N. Hacohen, Defining T Cell States
1178 Associated with Response to Checkpoint Immunotherapy in Melanoma. *Cell* **175**, 998-
1179 1013.e20 (2018).

1180 39. S. Kurtulus, A. Madi, G. Escobar, M. Klapholz, J. Nyman, E. Christian, M. Pawlak, D.
1181 Dionne, J. Xia, O. Rozenblatt-Rosen, V. K. Kuchroo, A. Regev, A. C. Anderson,
1182 Checkpoint Blockade Immunotherapy Induces Dynamic Changes in PD-1-CD8+ Tumor-
1183 Infiltrating T Cells. *Immunity* **50**, 181-194.e6 (2019).

1184 40. I. Siddiqui, K. Schaeuble, V. Chennupati, S. A. Fuertes Marraco, S. Calderon-Copete,
1185 D. Pais Ferreira, S. J. Carmona, L. Scarpellino, D. Gfeller, S. Pradervand, S. A. Luther,
1186 D. E. Speiser, W. Held, Intratumoral Tcf1+PD-1+CD8+ T Cells with Stem-like Properties
1187 Promote Tumor Control in Response to Vaccination and Checkpoint Blockade
1188 Immunotherapy. *Immunity* **50**, 195-211.e10 (2019).

1189 41. P. Ogilvie, G. Bardi, I. Clark-Lewis, M. Baggiolini, M. Uguccioni, Eotaxin is a natural
1190 antagonist for CCR2 and an agonist for CCR5. *Blood* **97**, 1920–1924 (2001).

1191 42. S. J. Cook, Q. Lee, A. C. Wong, B. C. Spann, J. N. Vincent, J. J. Wong, A. Schlitzer, M.
1192 D. Gorrell, W. Weninger, B. Roediger, Differential chemokine receptor expression and
1193 usage by pre-cDC1 and pre-cDC2. *Immunol Cell Biol* **96**, 1131–1139 (2018).

1194 43. M. T. Chow, A. J. Ozga, R. L. Servis, D. T. Frederick, J. A. Lo, D. E. Fisher, G. J.
1195 Freeman, G. M. Boland, A. D. Luster, Intratumoral Activity of the CXCR3 Chemokine
1196 System Is Required for the Efficacy of Anti-PD-1 Therapy. *Immunity* **50**, 1498-1512.e5
1197 (2019).

1198 44. D. Dangaj, M. Bruand, A. J. Grimm, C. Ronet, D. Barras, P. A. Duttagupta, E. Lanitis, J.
1199 Duraiswamy, J. L. Tanyi, F. Benencia, J. Conejo-Garcia, H. R. Ramay, K. T. Montone,
1200 D. J. Powell, P. A. Gimotty, A. Facciabene, D. G. Jackson, J. S. Weber, S. J. Rodig, S.
1201 F. Hodi, L. E. Kandalaft, M. Irving, L. Zhang, P. Foukas, S. Rusakiewicz, M. Delorenzi,
1202 G. Coukos, Cooperation between Constitutive and Inducible Chemokines Enables T
1203 Cell Engraftment and Immune Attack in Solid Tumors. *Cancer Cell* **35**, 885-900.e10
1204 (2019).

1205 45. N. Legrand, N. D. Huntington, M. Nagasawa, A. Q. Bakker, R. Schotte, H. Strick-
1206 Marchand, S. J. de Geus, S. M. Pouw, M. Böhne, A. Voordouw, K. Weijer, J. P. Di
1207 Santo, H. Spits, Functional CD47/signal regulatory protein alpha (SIRP(alpha))
1208 interaction is required for optimal human T- and natural killer- (NK) cell homeostasis in
1209 vivo. *Proc Natl Acad Sci U S A* **108**, 13224–13229 (2011).

1210 46. Y. Li, J.-J. Mention, N. Court, G. Masse-Ranson, A. Toubert, H. Spits, N. Legrand, E.
1211 Corcuff, H. Strick-Marchand, J. P. Di Santo, A novel Flt3-deficient HIS mouse model
1212 with selective enhancement of human DC development. *Eur J Immunol* **46**, 1291–1299
1213 (2016).

1214 47. P. See, C. A. Dutertre, J. Chen, P. Gunther, N. McGovern, S. E. Irac, M. Gunawan, M.
1215 Beyer, K. Handler, K. Duan, H. R. B. Sumatoh, N. Ruffin, M. Jouve, E. Gea-Mallorqui,
1216 R. C. M. Hennekam, T. Lim, C. C. Yip, M. Wen, B. Malleret, I. Low, N. B. Shadan, C. F.
1217 S. Fen, A. Tay, J. Lum, F. Zolezzi, A. Larbi, M. Poidinger, J. K. Y. Chan, Q. Chen, L.

Renia, M. Haniffa, P. Benaroch, A. Schlitzer, J. L. Schultze, E. W. Newell, F. Ginhoux, Mapping the human DC lineage through the integration of high-dimensional techniques. *Science* **356** (2017).

48. A. C. Villani, R. Satija, G. Reynolds, S. Sarkizova, K. Shekhar, J. Fletcher, M. Griesbeck, A. Butler, S. Zheng, S. Lazo, L. Jardine, D. Dixon, E. Stephenson, E. Nilsson, I. Grundberg, D. McDonald, A. Filby, W. Li, P. L. De Jager, O. Rozenblatt-Rosen, A. A. Lane, M. Haniffa, A. Regev, N. Hacohen, Single-cell RNA-seq reveals new types of human blood dendritic cells, monocytes, and progenitors. *Science* **356** (2017).

49. R. Bill, P. Wirapati, M. Messemaker, W. Roh, B. Zitti, F. Duval, M. Kiss, J. C. Park, T. M. Saal, J. Hoelzl, D. Tarussio, F. Benedetti, S. Tissot, L. Kandalaft, M. Varrone, G. Ciriello, T. A. McKee, Y. Monnier, M. Mermod, E. M. Blaum, I. Gushterova, A. L. K. Gonye, N. Hacohen, G. Getz, T. R. Mempel, A. M. Klein, R. Weissleder, W. C. Faquin, P. M. Sadow, D. Lin, S. I. Pai, M. Sade-Feldman, M. J. Pittet, CXCL9:SPP1 macrophage polarity identifies a network of cellular programs that control human cancers. *Science* **381**, 515–524 (2023).

50. J. Bae, L. Liu, C. Moore, E. Hsu, A. Zhang, Z. Ren, Z. Sun, X. Wang, J. Zhu, J. Shen, J. Qiao, Y.-X. Fu, IL-2 delivery by engineered mesenchymal stem cells re-invigorates CD8+ T cells to overcome immunotherapy resistance in cancer. *Nat Cell Biol* **24**, 1754–1765 (2022).

51. D. Voehringer, H.-E. Liang, R. M. Locksley, Homeostasis and effector function of lymphopenia-induced “memory-like” T cells in constitutively T cell-depleted mice. *J Immunol* **180**, 4742–4753 (2008).

52. P. Bourdely, G. Anselmi, K. Vaivode, R. N. Ramos, Y. Missolo-Koussou, S. Hidalgo, J. Tosselo, N. Nunez, W. Richer, A. Vincent-Salomon, A. Saxena, K. Wood, A. Lladser, E. Piaggio, J. Helft, P. Guermonprez, Transcriptional and Functional Analysis of CD1c(+) Human Dendritic Cells Identifies a CD163(+) Subset Priming CD8(+)CD103(+) T Cells. *Immunity* **53**, 335-352 e8 (2020).

53. F. Laforêts, E. Donnadieu, F. Balkwill, Protocol for real-time monitoring of CD8+ T and myeloid cell behavior in human high-grade serous ovarian cancer slices. *STAR Protocols* **5**, 103102 (2024).

Acknowledgments

We would like to thank the flow cytometry and the animal facility platforms from the CRI (Centre de Recherche sur l’Inflammation, Faculté de Médecine, Bichat) and from Pasteur Institute. We thank Rémy Yim, the human disease models core facility (Institut Pasteur, Paris) and the CRB de la Banque de Sang de Cordon, AP-HP, Paris for the experiments on the BRGSF reconstituted mice. We thank the units U1149 and U1016 of Institut National de la Santé et de la Recherche Médicale. We thank unit UMR3738 of Centre National de la Recherche at Pasteur Institute.

Funding

PG is a CNRS investigator (Centre National de la Recherche Scientifique)

Fonds National Suisse SINGERGIA SNF CRSII5_202246/1

INSERM transfert CO-POC grant

Agence Nationale pour la Recherche (ANR-17-CE11-0001-01 and ANR-18-IDEX-0001).

La Ligue contre le cancer Ile de France

Institut National du Cancer INCA (PL-BIO22-147)

Fondation pour la Recherche Médicale (EQU202203014687)

Fondation pour la Recherche sur le Cancer ARC (PJA2021060003913)

Author contributions

Conceptualization: PG, SH, JDS

Methodology: LG, FLRDC, PB, PG

Investigation: LG, FLRDC, PB, JB, NV, MV, AS, AO, OF, MA, HT, GA, FF

Resources: MC, JC, FG, LS, JH, MD, MD, JDS, SH, PG

Writing: LG, FLRDC, PG

Supervision: SH, PG

Funding acquisition: JH, SH, PG

Competing interests

The authors declare no competing interests. Patent Engraftment of mesenchymal stromal cells engineered to stimulate immune infiltration in tumors. EP23305569